JYX
JYVÄSKYLÄN YLIOPISTO
UNIVERSITY OF JYVÄSKYLÄ

This is a self-archived version of an original article. This version may differ from the original in pagination and typographic details.

Author(s): Hizbullah, Lintang; Rahaman, Ahibur; Safavi, Seyedeh; Haukka, Matti; Tocher, Derek A.; Lisensky, George C.; Nordlander, Ebbe

Title: Synthesis of phosphine derivatives of [Fe2(CO)6(μ-sdt)] (sdt = SCH2SCH2S) and investigation of their proton reduction capabilities

Year: 2023

Version: Published version

Copyright: © 2023 The Authors. Published by Elsevier Inc.

Rights: CC BY 4.0

Rights url: https://creativecommons.org/licenses/by/4.0/

Please cite the original version:

Hizbullah, L., Rahaman, A., Safavi, S., Haukka, M., Tocher, D. A., Lisensky, G. C., & Nordlander, E. (2023). Synthesis of phosphine derivatives of [Fe2(CO)6(μ-sdt)] (sdt = SCH2SCH2S) and investigation of their proton reduction capabilities. Journal of Inorganic Biochemistry, 246, Article 112272. https://doi.org/10.1016/j.jinorgbio.2023.112272

Journal of Inorganic Biochemistry 246 (2023) 112272

Contents lists available at ScienceDirect

Journal of Inorganic Biochemistry

journal homepage: www.elsevier.com/locate/jinorgbio

Synthesis of phosphine derivatives of $[Fe_2(CO)_6(\mu\text{-sdt})]$ (sdt = SCH_2SCH_2S) and investigation of their proton reduction capabilities

Lintang Hizbullah [a], Ahibur Rahaman [a,*,1], Seyedeh Safavi [a], Matti Haukka [b], Derek A. Tocher [c], George C. Lisensky [d], Ebbe Nordlander [a,*]

[a] Chemical Physics, Department of Chemistry, Lund University, Box 120, SE-221 00 Lund, Sweden
[b] Department of Chemistry, University of Jyväskylä, Box 111, FI-40014 Jyväskylä, Finland
[c] Department of Chemistry, University College London, Gower Street, London WC1E 6BT, UK
[d] Department of Chemistry, Beloit College, Beloit, WI 53511, USA

ARTICLE INFO

Keywords:
Hydrogenase
Iron carbonyl complex
Phosphine
Proton reduction
Cyclic voltammetry
Electrocatalysis

ABSTRACT

The reactions of $[Fe_2(CO)_6(\mu\text{-sdt})]$ (**1**) (sdt = SCH_2SCH_2S) with phosphine ligands have been investigated. Treatment of **1** with dppm (bis(diphenylphosphino)methane) or dcpm (bis(dicyclohexylphosphino)methane) affords the diphosphine-bridged products $[Fe_2(CO)_4(\mu\text{-sdt})(\mu\text{-dppm})]$ (**2**) and $[Fe_2(CO)_4(\mu\text{-sdt})(\mu\text{-dcpm})]$ (**3**), respectively. The complex $[Fe_2(CO)_4(\mu\text{-sdt})(\kappa^2\text{-dppv})]$ (**4**) with a chelating diphosphine was obtained by reacting **1** with dppv (*cis*-1,2-bis(diphenylphosphino)ethene). Reaction of **1** with dppe (1,2-bis(diphenylphosphino) ethane) produces $[\{Fe_2(CO)_4(\mu\text{-sdt})\}_2(\mu\text{-}\kappa^1\text{-dppe})]$ (**5**) in which the diphosphine forms an intermolecular bridge between two diiron cluster fragments. Three products were obtained when dppf (1,1′-bis(diphenylphosphino) ferrocene) was introduced to complex **1**; they were $[Fe_2(CO)_5(\mu\text{-sdt})(\kappa^1\text{-dppfO})]$ (**6**), the previously known $[\{Fe_2(CO)_5(\mu\text{-sdt})\}_2(\mu\text{-}\kappa^1\text{-}\kappa^1\text{-dppf})]$ (**7**), and $[Fe_2(CO)_4(\mu\text{-sdt})(\mu\text{-dppf})]$ (**8**), with complex **8** being produced in highest yield. Single crystal X-ray diffraction analysis was performed on compounds **2**, **3** and **8**. All structures reveal the adoption of an *anti*-arrangement of the dithiolate bridges, while the diphosphines occupy dibasal positions. Infra-red spectroscopy indicates that the mono-substituted complexes **5**, **6**, and **7** are inert to protonation by HBF_4Et_2O, but complexes **2**, **3**, **4** and $[Fe_2(CO)_5(\mu\text{-sdt})(\kappa^1\text{-}PPh_3)]$ (**9**) show shifts of their $\nu_{(C\text{-}O)}$ resonances that indicate that protons bind to the metal cores of the clusters. Addition of the one-electron oxidant $[Cp_2Fe]PF_6$ does not lead to any discernable shift in the IR resonances. The redox chemistry of the complexes was investigated by cyclic voltammetry, and the abilities of complexes to catalyze electrochemical proton reduction were examined.

1. Introduction

In biological systems, the redox chemistry in the production and utilization of H_2 is catalyzed by enzymes called hydrogenases (H_2ases). The hydrogenase enzymes catalyze both uptake and production of hydrogen, i.e. $H_2 \rightarrow 2H^+ + 2e^-$ (hydrogen oxidation) or the reverse reaction (proton reduction), depending upon the conditions [1–4]. These enzymes are classified into three major families on the basis of the metal content in their active sites, and have been identified in archaea, bacteria, and eucarya [5,6]. The class known as [FeFe] hydrogenases catalyzes proton reduction and demonstrates the highest turnover numbers and frequencies for H_2 production of all hydrogenase enzymes. The characteristic structure of an [FeFe] H_2ase active site was first revealed by determination of the crystal structure of the enzyme from *Clostridium pasteurianum* [7,8] (Fig. 1). The site consists of two components: a [4Fe—4S] ferredoxin cubane cluster that is linked by a 12.5 Å

Abbreviations: sdt, sulfur dithiolato; edt, 1,2-ethane dithiolato; adt, aza dithiolato; pdt, 1,3-propane dithiolato; odt, oxa dithiolato; TTL, 1,2,4-trithiolane; dppm, diphenyl phosphino methane; dcpm, dicyclohexyl phosphino methane; dppv, *cis*-1,2-bis(diphenylphosphino)ethene; dppe, diphenyl phosphino ethane; dppf, 1,1′-bis (diphenylphosphine)ferrocenyl; PPh_3, triphenylphosphine; CO, carbonyl; CN, nitrile; Me_3NO, trimethyl amine *N*-oxide; CH_3CN, acetonitrile; CH_2Cl_2, dichloromethane; *p*-TsOH, *p*-toluenesulfonic acid; THF, tetrahydrofuran; FTIR, Fourier transform infra-red; NMR, nuclear magnetic resonance; MHz, megahertz.

* Corresponding authors.
E-mail addresses: Ahibur.rahaman@su.se (A. Rahaman), ebbe.nordlander@chemphys.lu.se (E. Nordlander).
[1] Present Address: Department of Organic Chemistry, Arrhenius Laboratory, Stockholm University, Svante Arrhenius väg 16C, 10,691 Stockholm, Sweden

https://doi.org/10.1016/j.jinorgbio.2023.112272
Received 8 December 2022; Received in revised form 10 April 2023; Accepted 28 May 2023
Available online 7 June 2023
0162-0134/© 2023 The Authors. Published by Elsevier Inc. This is an open access article under the CC BY license (http://creativecommons.org/licenses/by/4.0/).

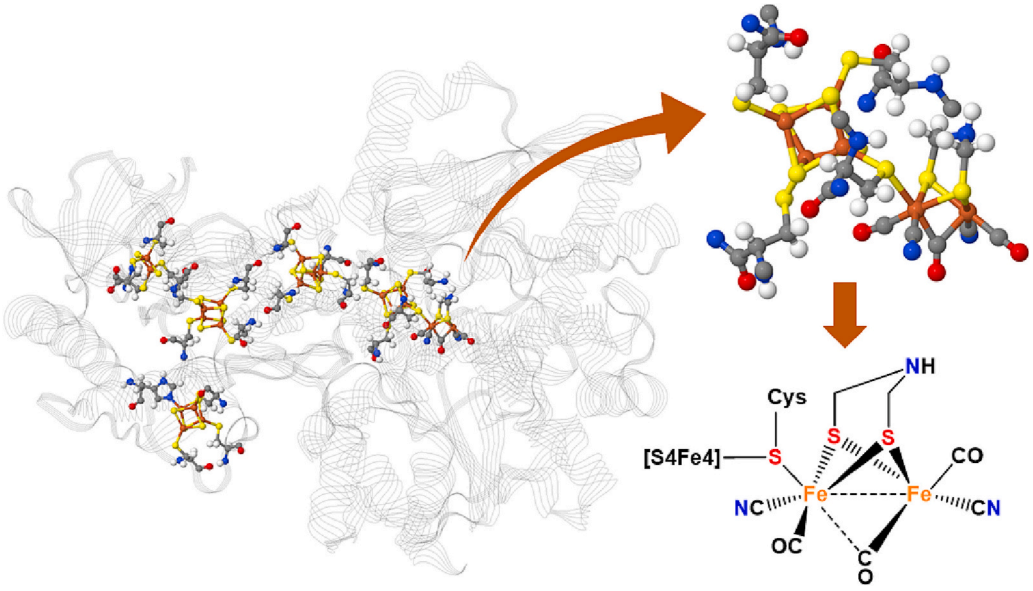

Fig. 1. Schematic drawing of the structure of the *Clostridium pasteurianum* [Fe-Fe] hydrogenase [7,8], highlighting the chain of Fe-S electron transfer sites leading to the H-cluster, the active site for proton reduction/hydrogen oxidation.

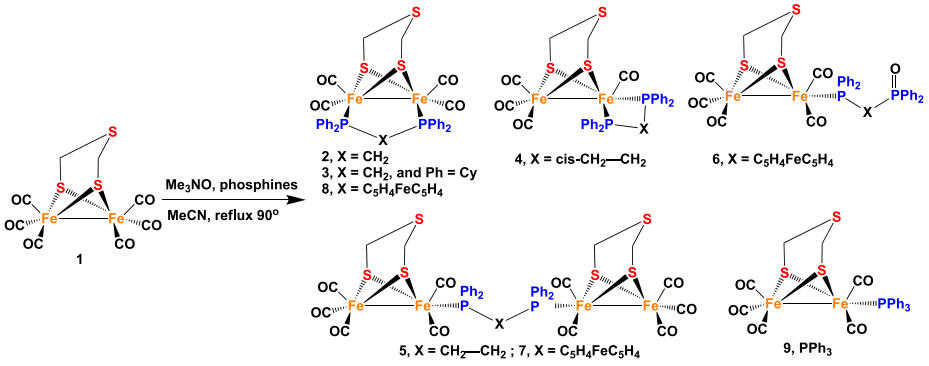

Scheme 1. Schematic depiction of the syntheses of clusters **2–9** from the starting material $[Fe_2(CO)_6(\mu\text{-sdt})]$ (**1**). Clusters **7** and **9** are known previously [41].

protein backbone to the catalytic diiron unit, which is bridged by a dithiolate ligand (Fig. 1). This active site is called the H-cluster, and the diiron unit is called the $[2Fe]_H$ sub-cluster. The active site is buried deep inside the protein and connected to an electron transfer pathway involving several iron-sulfur clusters (Fig. 1). The ligand coordination in the $[2Fe]_H$ sub-cluster consists of two square pyramidal iron ions that are antisymmetric with respect to each other and that together are coordinated by five carbon-based diamagnetic π-acceptor ligands (CO and CN^-) that stabilize the low oxidation states of the metals, in addition to the dithiolate bridge. One of the carbonyl ligands is bound in a semi-bridging coordination mode between the two iron centers, which results in a vacant terminal coordination site on one iron ion (the distal iron) that may be coordinated by a replaceable ligand (e.g. H_2O or H_2, Fig. 1) [9,10].

Dithiolate-bridged diiron complexes have been used extensively to mimic the $[2Fe]_H$ subcluster found in [Fe-Fe]-hydrogenases [11–18]. Many such diiron dithiolate complexes have been found to perform electrocatalytic proton reduction [11] but unfortunately these electrocatalysts suffer from high overpotentials and poor turnover numbers and frequencies, unlike platinum-based compounds that can effectively catalyze the reaction [19]. However, the desire to develop effective, environmentally benign and cheap catalysts for proton reduction means that there is still considerable scope for the development of effective biomimetic catalysts for this reaction.

Weigand and coworkers have reported the synthesis and characterization of the complex $[Fe_2(CO)_6(\mu\text{-sdt})]$ (**1**) (sdt = SCH_2SCH_2S) [20]. The reaction of diiron nonacarbonyl with 1,2,4-trithiolane was found to yield **1**, with the trithiolane ligand adopting similar structure to that found for the aza-dithiolate (adt) [12], 1,3-propane-dithiolate (pdt) [13], and oxa-dithiolate (odt) [15] analogues. The presence of the additional sulfide in the trithiolane ligand offers, potentially, a new/additional protonation site that differs or is absent from those present in the adt/pdt/odt analogues of **1**. Compound **1** shows electrochemical reduction through two reversible one-electron steps in CH_3CN, $[FeFe]^-$ at −1.505 V and $[FeFe]^{2-}$ at −1.39 V in CH_3CN [20]. When pivalic acid was introduced, the chemical reversibility of these redox waves was found to disappear [20]. Weigand and coworkers suggested that the acidity of pivalic acid was insufficient for catalytic hydrogen generation at the above-mentioned reduction potentials. Instead, modelling suggests that two molecules of pivalic acid bind to the doubly reduced anion $[FeFe]^{2-}$ (or that proton transfer to generate neutral diiron species occurs). Subsequent formation of hydride species is formed in two steps at lower (more negative) potentials. Catalytic hydrogen generation was proposed to occur in concert with an irreversible charge transfer reaction [20].

Possible ways to alter and improve catalytic hydrogen evolution based on **1** could be to use a Brönsted acid with lower pK_a and/or to render the complex more susceptible to protonation (at the iron core) by

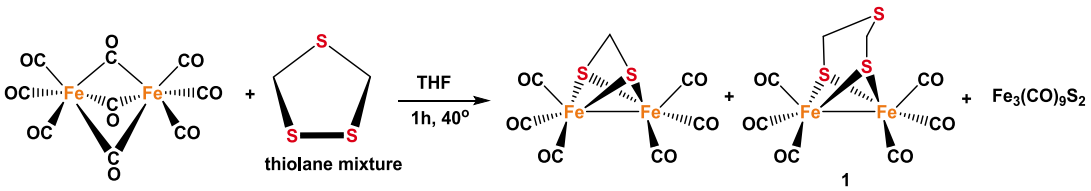

Scheme 2. Formation of the parent complex [($Fe_2(CO)_6$(μ-sdt)] (**1**) from the 1,2,4-trithiolane ligand. A fourth, unidentified, product is formed in the reaction (see text).

substitution of the carbonyl ligands with less π-acidic ligands, e.g. phosphines. Phosphine substitution is expected to increase the electron density on the cluster metal core, and thus make the cluster more susceptible to protonation at the metals [21,22]. We have prepared a number of phosphine derivatives of **1**. In order to vary both electronic influence and coordination modes of the ligands, we chose phosphines of varying basicity that were expected to coordinate in a chelating manner to one iron ion (dppm, dcpm, dppv), or a bridging coordination mode (dppf). The latter ligand also provides a (potential) additional metal-based redox center. Herein we present the synthesis, characterization and electrochemical behavior of [$Fe_2(CO)_4$(μ-sdt)(μ-dppm)] (**2**), [$Fe_2(CO)_4$(μ-sdt)(μ-dcpm)] (**3**), [$Fe_2(CO)_4$(μ-sdt)(κ^2-dppv)] (**4**), [{$Fe_2(CO)_5$(μ-sdt)}$_2$(μ-κ^1-κ^1-dppe)] (**5**), [$Fe_2(CO)_5$(μ-sdt)(κ^1-dppfO)] (**6**), [{$Fe_2(CO)_5$(μ-sdt)}$_2$(μ-κ^1-κ^1-dppf)] (**7**), [$Fe_2(CO)_4$(μ-sdt)(*μ*-dppf)] (**8**), and [$Fe_2(CO)_5$(μ-sdt)(PPh_3)] (**9**). (Scheme 1). The synthesis and characterization of complexes **7** and **9** have been described earlier by Song and coworkers [41]. The abilities of clusters **2**–**9** to act as catalysts for the electrochemical reduction of protons provided from *p*-toluenesulfonic acid (*p*-TsOH) have been studied. By using different phosphine ligands, we were able to vary the electron densities in the diiron cores of the clusters, increasing their electrocatalytic proton reduction capabilities.

2. Experimental

2.1. General procedures

All reactions were carried out under nitrogen atmosphere using standard Schlenk techniques unless otherwise stated. Reagent-grade solvents were dried prior to use. The starting materials [$Fe_2(CO)_9$], $Na_2S{\cdot}9H_2O$, elemental sulfur, trimethyl amine N-oxide (Me_3NO), and the phosphine ligands were purchased from Sigma Aldrich and used as received. Infrared spectra were recorded on an Agilent Technologies Cary 630 FTIR instrument. NMR spectra were recorded on Bruker Avance II 500 MHz and Bruker BioSpin 400 MHz spectrometers. Preparative thin-layer chromatography was carried out on silica gel GF254 (type 60, E. Merck). Microanalyses were performed by Mikroanalytisches Laboratorium Kolbe, Oberhausen, Germany.

2.2. Preparation of [$Fe_2(CO)_6$(*μ*-sdt)] (1)

The 1,2,4-trithiolane ligand was prepared following the procedure of Morita and Kobayashi [23] with modifications. Air was excluded from the system as much as possible. To a solution of degassed water (100 mL), 30 g of $Na_2S{\cdot}9H_2O$ was added and stirred until dissolution. To the same flask, 6 g of sulfur was added, and the mixture was stirred vigorously for 30 min. The solution changed color from pale yellow to red orange and the pH increased to above 12.7. The flask was charged with 130 mL of CH_2Cl_2 and the solution was stirred vigorously for 7 h. After the stirring was stopped, the solution was separated into two phases. The organic phase was washed thrice with degassed water and dried over anhydrous Na_2SO_4. The solvent was removed using a rotary evaporator. A yellow oily substance was obtained, which is a mixture of 1,2,4-trithiolane and another organosulfur polymer [23]. Because of the difficulty in separating these substances, a low yield of approximately 1.3% by weight of 1,2,4-trithiolane was assumed on the basis of an earlier report [24]. Into the flask that contained the mixture, tetrahydrofuran (THF, 30 mL) was added and stirred overnight. The THF solution was filtered through a cotton wad into another flask and charged with 2 g of [$Fe_2(CO)_9$]. This solution was stirred and gently heated at 40°C for about 1 h under nitrogen atmosphere [20]. The solvent was removed under reduced pressure and the crude product inside was scratched to release it from the wall of the round bottom flask. A total of 30 mL of hexane was added to the flask and the mixture was stirred for 3 h. The resultant solution was subsequently separated by silica gel column chromatography, using hexane as an eluent. Four bands were obtained but two of them remain unidentified. The first product appeared as a yellow band which turned green after long exposure to air, IR (ν_{CO}, pentane): 2081, 2041, 2002 cm^{-1} and no peaks detected by ^{1}H NMR (unidentified product). The second product was dark purple, IR (ν_{CO}, pentane): 2078, 2023, and 1988 cm^{-1}; ^{1}H NMR (500 MHz, $CDCl_3$): δ 4.63 (identified as the methylenedithiolato-bridged diiron complex ([$Fe_2(CO)_6$(μ-mdt)], mdt = SCH_2S, see Scheme 2, below) [25]. An amount of 220 mg of pure [$Fe_2(CO)_6$(μ-sdt)] (**1**) was obtained from the third band. ^{1}H NMR (500 MHz, $CDCl_3$): δ 3.21 (s), IR (ν_{CO}, pentane): 2078(s), 2040(s), 2001(s). The fourth (unidentified) product was dark red, IR (ν_{CO}, pentane): 2074 (s), 2035(s), 1998(s), and 1985(sh).

2.3. Synthesis of [$Fe_2(CO)_4$(*μ*-sdt)(*μ*-dppm)] (2)

To a CH_3CN solution (25 mL) of **1** (50 mg, 0.124 mmol) and 1,2-bis (diphenylphosphino)methane (47 mg, 0.124 mmol) in a round-bottom flask, a solution of Me_3NO (18 mg, 0.248 mmol) in the same solvent (10 mL) was added dropwise through an addition funnel. The solution was brought to reflux at 90°C and stirred for one hour. The solution was concentrated on a rotary evaporator and subjected to thin layer chromatography (TLC) using hexane:CH_2Cl_2 (3:2 v/v) as eluent. Two bands were developed, the faster moving band was tentatively assigned as [$Fe_2(CO)_5$(μ-sdt)(κ^1-dppm)] on the basis of its IR spectrum, which is similar to [$Fe_2(CO)_5$(μ-sdt)(κ^1-PPh_3)] [41]. (12 mg,13%) IR (ν_{CO}, CH_2Cl_2) 2046(s), 1983(s), and 1931(s) (no NMR was detected as the compound decomposed). The second band afforded [$Fe_2(CO)_4$(μ-sdt)(μ-dppm)] (**2**) (47 mg, 51.8%) as red orange crystals after recrystallization from hexane/CH_2Cl_2 at 4°C. **2** IR (ν_{CO}, CH_2Cl_2) 1989(m), 1955(s), 1910(s); ^{1}H NMR ($CDCl_3$): δ 7.69 (m, 20H), 3.73 (s, 2H), and 3.33 (s, 4H); ^{31}P{^{1}H}-NMR($CDCl_3$): δ 52.90 (s). HR-MS: *m/z* 732.9246 found, *m/z* 732.9232 calc for [M + H$^+$]. Anal. calc. (mass %) C 50.84 H 3.58 S 12.13 P 8.64; found C 50.75 H 3.51 S 12.85 P 8.49

2.4. Synthesis of [$Fe_2(CO)_4$(*μ*-sdt)(*μ*-dcpm)] (3)

A total of 50 mg of **1** (0.12 mmol) and 49 mg (0.124 mmol) of 1,2-bis (dicyclohexylphosphino)methane were dissolved in 20 mL of CH_3CN solvent. A solution of Me_3NO (18 mg, 0.248 mmol) in 10 mL of CH_3CN was added dropwise through an addition funnel. The solution was heated to reflux at 90°C and stirred for one hour. The solvent was removed on a rotary evaporator and the residue was chromatographed by TLC on silica gel using hexane:CH_2Cl_2 (3:2 v/v) as eluent. The sole product detected was a pale red band of [$Fe_2(CO)_4$(μ-sdt)(μ-dcpm)] (**3**) (45 mg, 48%), which was isolated as pale red crystals after

recrystallization from hexane/CH_2Cl_2 at 4°C. **3**, IR (ν_{CO}, CH_2Cl_2) 1981 (m), 1949(s), 1914(s); ^{1}H NMR ($CDCl_3$): δ 3.25 (4H, $J = 54.3$ Hz, d), 2.27 (2H, $J = 0.08$ Hz, d), 2.13 (d, $J = 0.03$, 2H), 1.86 (20H, m), 1.39 (10H, m), 1.28 (12H, m); ^{31}P{^{1}H}-NMR ($CDCl_3$): δ 60(s). HR-MS: *m/z* 757.1124 found, *m/z* 757.1132 calc for [M^+]. Anal. calc. (mass %) C 49.22 H 6.66 S 12.71 P 8.19; found C 48.95 H 6.46 S 12.44 P 8.04

2.5. Synthesis of [$Fe_2(CO)_4$(μ-sdt)(κ^2-dppv)] (4)

A total of 50 mg of **1** (0.124 mmol) and *cis*-1,2-bis(diphenylphosphino)ethene (49 mg, 0.124 mmol) in 30 mL of CH_3CN was inserted into a flask. A solution of Me_3NO (18 mg, 0.248 mmol) in 10 mL of CH_3CN was added dropwise into the flask via an addition funnel. The reaction mixture was refluxed at around 90°C for an hour and a half. The solvent was removed under reduced pressure and the residue was chromatographed by thin layer chromatography. Elution using hexane:CH_2Cl_2 (3:2 v/v) developed one band, [$Fe_2(CO)_4$(μ-sdt)(κ^2-dppv)] (**4**) (38 mg, 41.2%); IR (ν_{CO}, CH_2Cl_2), 2022(s), 1949(s), 1918(sh); ^{1}H NMR ($CDCl_3$): δ 7.77 (6H, m), 7.63 (4H, m), 7.44 (12H, m), 3.76 (4H, $J = 2.8$ Hz, d). ^{31}P{^{1}H}-NMR($CDCl_3$): δ 95 (s), 79 (s). HR-MS: *m/z* 744.9246 found, *m/z* 744.9251 calc for [$M + H^+$]. Anal. calc. (mass %) C 41.76 H 2.80 S 16.72 P 5.38; found C 40.87 H 3.07 S 16.54 P 5.12

2.6. Synthesis of [{$Fe_2(CO)_5$(μ-sdt)}$_2$(μ-κ^1-κ^{1}dppe)] (5)

A total of 50 mg of **1** (0.124 mmol) and 49 mg (0.124 mmol) of 1,2-bis(diphenylphosphino)ethane were dissolved in 25 mL of CH_3CN. A solution of 18 mg (0.248 mmol) of Me_3NO in 10 mL of CH_3CN were added through an addition funnel. The reaction mixture was refluxed at 90°C for an hour. The solution was concentrated on a rotary evaporator and subjected to TLC on silica gel using hexane:CH_2Cl_2 (3:2 *v*/v) as eluent. A sole product was isolated and identified as [{$Fe_2(CO)_5$(μ-sdt)}$_2$(μ-κ^1-κ^{1}dppe)] (**5**) (48 mg, 35.5%); IR (ν_{CO}, CH_2Cl_2) 2048(s), 1986 (s), 1963(m), and 1933(sm); ^{1}H NMR ($CDCl_3$): δ 7.46 (m, 20H), 2.82 (s, 8H), and 2.11 (s, 4H); ^{31}P{^{1}H}-NMR($CDCl_3$): δ 58.81 (s). HR-MS: *m/z* 1172.7090 found, *m/z* 1172.7081 calc for [$M + Na^+$]. Anal. calc. (mass %) C 41.76H 2.80 S 16.72 P 5.38; found C 40.87H 3.07 S 16.54 P 5.12

2.7. Reaction of [$Fe_2(CO)_4$(μ-sdt)] with dppf

A total of 50 mg of **1** (0.124 mmol) and 68 mg (0.124 mmol) of 1,2-*bis*(diphenylphosphino)ferrocene were dissolved in 30 mL of CH_3CN in a two-neck 50 mL round bottom flask. A solution of 18 mg (0.456 mmol) of Me_3NO dissolved in 10 mL of CH_3CN were added through an addition funnel under a nitrogen flow. The solution was heated to reflux at 90°C and stirred for two hours. The solution was concentrated on a rotary evaporator and subjected to column chromatography on silica gel using hexane:CH_2Cl_2 (3:2 v/v) as eluent. Three bands were developed – the fastest moving band was identified as [$Fe_2(CO)_5$(μ-sdt)(κ^1-dppfO)] (**6**) (17 mg, 14.5%), **6** IR (ν_{CO}, CH_2Cl_2) 2045(s), 2023(m), 1982(s), 1958(s), 1913(sh), 1892(w); ^{1}H NMR ($CDCl_3$): δ 7.51 (m, 20H), 4.67(s, 2H), 4.77 (s, 2H), and 4.30 (m, 8H); ^{31}P{^{1}H}-NMR ($CDCl_3$): δ 40.79 (s), 28.17 (s). HR-MS: *m/z* 968.8782 found, *m/z* 968.8789 calc for [$+Na^+$] Anal. calc. (mass %) C 52.04H 3.41 S 10.16 P 6.55; found C 51.56H 3.24 S 10.04 P 6.49; the second band was [{$Fe_2(CO)_5$(μ-sdt)}$_2$(μ-κ^1-κ^{1}dppf)] (**7**) [41] 18 mg (11.1%). **7** IR (ν_{CO}, CH_2Cl_2) 2046(s), 1984(s), 1968(sh), and 1930 (sm) cm^{-1}; ^{1}H NMR ($CDCl_3$): δ 7.44 (m, 20H), 4.67 (s, 4H), 4.77 (s, 4H), 4.21 (m, 8H); ^{31}P{^{1}H}-NMR ($CDCl_3$): δ 54.96 (s); HR-MS: *m/z* 1306.6933 found, *m/z* 1306.6935 calc for [$M + H^+$]; and the final band was identified as [$Fe_2(CO)_4$(μ-sdt)(μ-dppf)] (**8**) 21 mg (18.8%), which was isolated as red crystals after recrystallization from hexane/CH_2Cl_2 at 4°C. **8**: IR (ν_{CO}, CH_2Cl_2) 1989(s), 1955(s), 1922(s); ^{1}H NMR ($CDCl_3$): δ 7.51 (m, 20H), 4.66 (s, 2H), 4.53 (s, 2H), 4.15 (m, 8H); ^{31}P{^{1}H}-NMR ($CDCl_3$): δ 50.98(s); HR-MS: *m/z* 901.8986 found, *m/z* 901.8995 calc for [M^+]. Anal. calc. (mass %) C 53.22 H 3.57 S 10.66 P 6.87; found C 53.12 H 3.64 S 10.43 P 6.55

A table with comparison of spectroscopic data for complexes **2**–**8** with those of known and structurally related complexes is included in the Supplementary Material (Table S1).

2.8. X-ray diffraction studies

Single crystals of **2**, **3** and **8** suitable for X-ray diffraction were grown by slow diffusion of hexane into CH_2Cl_2 solutions at 4°C. Crystals were immersed in cryo-oil, mounted on a Nylon loop, and measured at a temperature of 120–170 K. The X-ray diffraction data were collected on a Bruker Kappa Apex II Duo diffractometer using Mo Kα radiation (λ = 0.71073 Å). The CrysAlisPro [26] program package was used for cell refinements and data reductions. Structures were solved by direct methods or by charge flipping using the SHELXL-2017/1 [27] programs. A multi-scan, numerical, or Gaussian absorption correction (CrysAlisPro [26]) was applied to all data. Structural refinements were carried out using SHELXL-2017/1 [27]. The hydrogen atoms were positioned geometrically and constrained to ride on their parent atoms, with C-H = 0.95–0.99 Å and $U_{iso} = 1.2\ U_{eq}$ (parent atom).

2.9. Protonation of diiron clusters

A small amount of each diiron cluster (1.9–2.1 mg) was dissolved in CH_2Cl_2 at room temperature. The solutions were acidified with 1 M equivalents of HBF_4Et_2O or *p*-tolylsulfonic acid (tosylic acid, *p*-TsOH). The resultant acid-containing solution was transferred into an IR cell and a series of spectra were recorded over time.

2.10. Oxidation of diiron clusters

1 M equivalent of [Cp_2Fe](PF_6) (0.9 mg, 2.5×10^{-3} mmol) was dissolved in 0.5 mL of a CH_2Cl_2 solution containing the diiron complex. The mixture was immediately transferred to an IR cell and monitored over time. No significant changes in the IR spectrum were noted.

2.11. Electrochemistry

A solution of 0.1 M [n-Bu_4N][PF_6] in anhydrous CH_3CN (Fisher Chemical, HPLC Grade) was used as electrolyte in all cyclic voltammetry experiments. Electrochemical measurements were performed using either a PalmSens4 potentiostat and PSTrace 5.8 software or PineWaveNow potentiostat and AfterMath software. All voltammograms were obtained under a N_2 atmosphere using a cell with a 2 or 3 mm diameter glassy carbon working electrode, a platinum counter electron, and an Ag/Ag^+ (0.005 or 0.01 M AgCl/0.1 M n-Bu_4NPF_6 in MeCN) reference electrode. All potentials are quoted against the ferrocene/ferrocenium (Fc/Fc^+) potential run as an internal standard.

3. Results and discussion

3.1. Preparation of 1,2,4-trithiolane

The 1,2,4-trithiolane was synthesized following the procedure of Morita and Kobayashi [23] (cf. Experimental Section). Separation by column chromatography using silica gel (9:1 hexane:CH_2Cl_2) was performed and pure product was obtained, but the yield was so minuscule that the collected product was used only for characterization via ^{1}H NMR. A singlet peak was detected at 4.21 ppm, which matches with the literature [23]. Isolation and preservation of the product is impractical as the compound tends to decompose and polymerize in the presence of air. The trithiolane ligand needs to be stored under an inert atmosphere inside a − 80°C fridge to preserve the pure compound [24]. Therefore, the crude product was used without further purification in the subsequent metalation reaction.

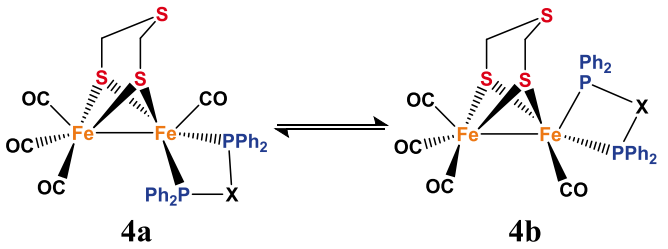

Fig. 2. Two isomers of $[Fe_2(CO)_4(\mu\text{-sdt})(\kappa^2\text{-dppv})]$ (**4**) present in solution: (**4a**) dibasal and (**4b**) basal-apical conformation.

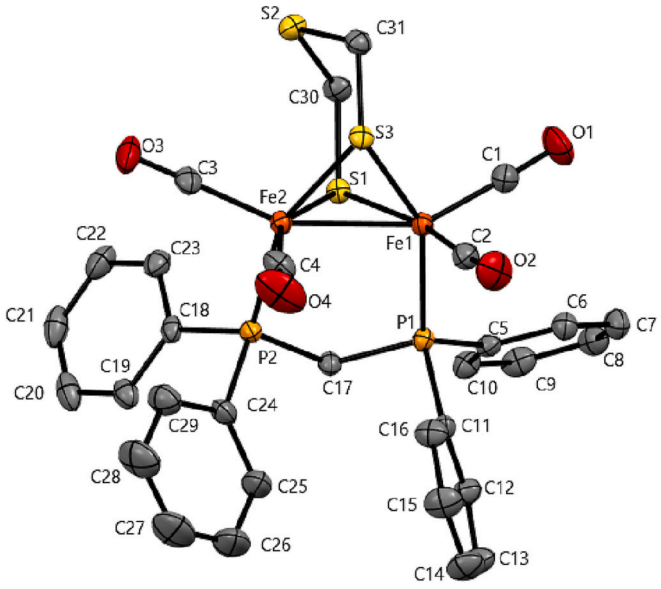

Fig. 3. Solid state molecular structure of $[Fe_2(CO)_4(\mu\text{-sdt})(\mu\text{-dppm})]$ (**2**). Ring hydrogen atoms are omitted for clarity. Selected bond distances (Å) and angles (°): Fe(1)-Fe(2) 2.5058(4), Fe(1)-S(1) 2.2651(6), Fe(1)-S(3) 2.2499(6), Fe(1)-P(1) 2.2553(7), Fe(2)-P(2) 2.2179(6), Fe(2)-S(1) 2.2751(6), Fe(2)-S(3) 2.2537(6), Fe(2)-Fe(1)-S(1) 56.69(2), Fe(2)-Fe(1)-S(3) 56.27(2), Fe(2)-Fe(1)-P(1) 94.47(2), Fe(1)-Fe(2)-P(2) 99.51(2), Fe(2)- *S*(1)-Fe(1) 67.00(2), Fe(2)-*S*(3)-Fe(1) 67.61(2), Fe(2)-Fe(1)-C(1) 148.61(8), Fe(2)-Fe(1)-C(2) 108.12(8).

3.2. Preparation of $[Fe_2(CO)_6(\mu\text{-sdt})]$ (1)

Triiron dodecarbonyl has been reported as an iron source that can react with trithiolane (sdt) to form $[Fe_2(CO)_6(\mu\text{-sdt})]$ (**1**) [28]. An attempt was made to use the triiron complex as starting material for the synthesis of **1** but several difficulties arose due to the number of products obtained in the reaction and the impracticality of later separation of the mixture. Therefore, only diiron nonacarbonyl was used as the iron source for complexation. The reaction was carried out under the conditions shown in Scheme 2 with direct metalation of the crude trithiolane mixture [20]. The optimum reaction conditions were found to be gentle heating at 40°C in THF for about one hour with stirring, for the ligand to completely coordinate to the metal complex. A large excess of unreacted ligand was polymerized, producing a rubber-like side product. After scratching the reaction flask, the mixture was immersed in hexane because the targeted iron carbonyl products can be dissolved in hexane while other compounds in the reaction mixture only dissolved in CH_2Cl_2.

Separation of the mixture was achieved by silica gel column chromatography in hexane, giving four different iron complexes (Scheme 2). The first eluate remains unidentified (see Experimental Section). The second eluate came out close to the first product. The eluate solution has a dark purple color and exhibits IR $\nu_{(C\text{-}O)}$ absorptions at 2078, 2023, and

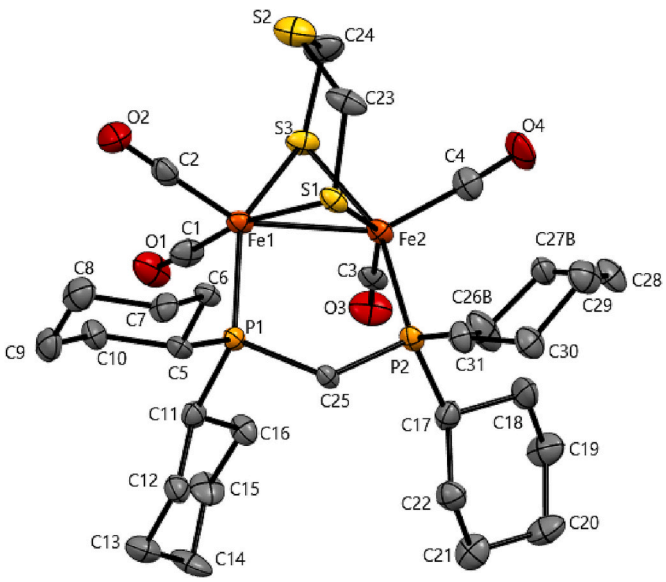

Fig. 4. Solid state molecular structure of $[Fe_2(CO)_4(\mu\text{-sdt})(\mu\text{-dcpm})]$ (**3**). Ring hydrogen atoms are omitted for clarity. Selected bond distances (Å) and angles (°): Fe(1)-Fe(2) 2.531(2), Fe(1)-S(1) 2.256(2), Fe(1)-S(3) 2.252(2), Fe(1)-P(1) 2.245(2), Fe(2)-P(2) 2.255(3), Fe(2)-S(1) 2.263(2), Fe(2)-S(3) 2.230(2), Fe(2)-Fe(1)-S(1) 56.06(6), Fe(2)-Fe(1)-S(3) 55.22(6), Fe(2)-Fe(1)-P(1) 94.33(7), Fe(1)-Fe(1)-P(2) 101.07(7), Fe(2)- *S*(1)-Fe(1) 68.12(7), Fe(2)- *S*(3)-Fe(1) 68.76(7), Fe(2)-Fe(1)-C(1) 109.1(3), Fe(2)-Fe(1)-C(2) 149.0(3).

1988 cm^{-1}, indicating a diiron complex. The ^1H NMR spectrum showed a singlet at 4.6 ppm, matching the literature value of the known methylenedithiolato-bridged diiron side product [25].

The third band is the major and desired product, eluting as a clean red orange solution with IR absorptions at 2078, 2040, and 2001 cm^{-1} and a singlet in the ^1H NMR spectrum at 3.2 ppm that matches the literature values for $[Fe_2(CO)_6(\mu\text{-sdt})]$ (**1**) [20]. The last eluent appeared at a slow pace with dark red color, showing IR resonances at 2074, 2035, 1998, and a shoulder at 1985 cm^{-1} and no ^1H NMR peak, which closely resemble the data for $[Fe_3(CO)_9S_2]$, although further characterization is needed [29].

3.3. Synthesis of phosphine derivatives

When the parent compound **1** had been obtained, a number of phosphine derivatives (didentate diphosphine = dppm, dcpm, dppe, dppv, dppf, and monodentate PPh_3) were prepared under similar conditions as those used for preparing diphosphine derivatives of similar dithiolate bridged diiron complexes, e.g. $[Fe_2(CO)_6(\mu\text{-edt})]$ and $[(Fe_2(CO)_6(\mu\text{-pdt})]$ (pdt = propane dithiolate; edt = ethane dithiolate) [30]. The reactions yielded the complexes **2**–**9**, all of which have been characterized by IR, ^1H, and ^{31}P NMR spectroscopies and mass spectrometry. In the cases of **2**, **3** and **8**, their structures have been confirmed by single crystal X-ray crystallography. Complexes **7** and **9** have been published earlier by Song and coworkers [41].

3.3.1. Intramolecular bridging coordination of diphosphines

Reacting a solution of **1** with dppm or dcpm at elevated temperature (90°C) yields complexes $[Fe_2(CO)_4(\mu\text{-sdt})(\mu\text{-dppm})]$ (**2**) and $[Fe_2(CO)_4(\mu\text{-sdt})(\mu\text{-dcpm})]$ (**3**), respectively, as sole products. Treatment of **1** with dppf resulted in the formation of several complexes, including $[Fe_2(CO)_4(\mu\text{-sdt})(\mu\text{-dppf})]$ (**8**). The structural similarities of **2**, **3**, and **8** are indicated by their strong and sharp IR absorption patterns in the $\nu_{(C—O)}$ region, at 1989(m), 1955(s), and 1910(s) cm^{-1} for **2**, at 1981(m), 1949(s), and 1914(s) cm^{-1} for **3**, and 1989(m), 1955(s), and 1922(s) cm^{-1} for **8**. A shift to lower frequencies by approximately 10–50 cm^{-1} was thus observed upon substitution of two carbonyls of **1** ($\nu_{(C—O)}$ 2078

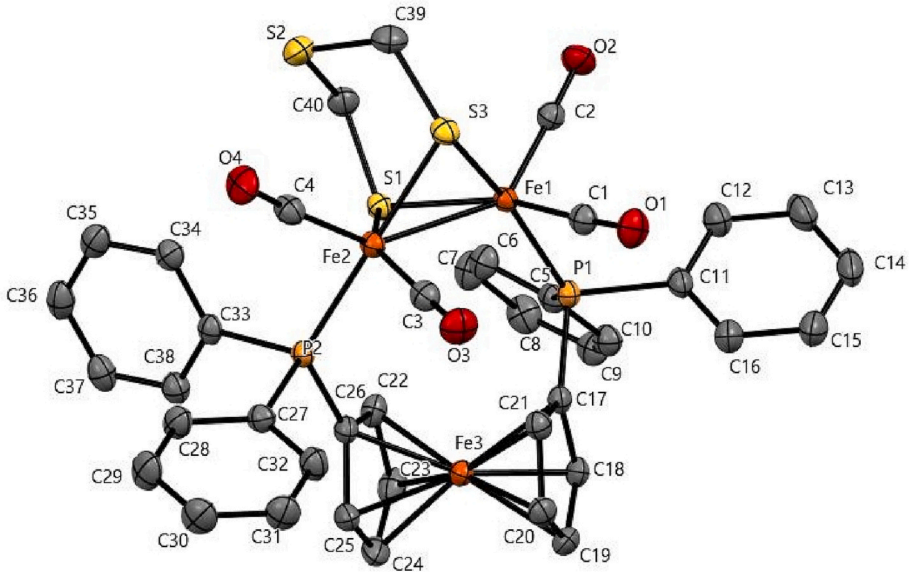

Fig. 5. Solid state molecular structure of $[Fe_2(CO)_4(\mu\text{-sdt})(\mu\text{-dppf})]$ (**8**). Ring hydrogen atoms are omitted for clarity. Selected bond distances (Å) and angles (°): Fe(1)-Fe(2) 2.6402(6), Fe(1)-P(1) 2.2621(6), Fe(2)-P(2) 2.2379(5), Fe(1)-S(1) 2.2551 (5), Fe(1)-S(3) 2.2597(6), Fe(2)-S(1) 2.2512(6), Fe (2)-S(3) 2.2416(5; Fe(2)-Fe(1)-S(1) 54.07(1), Fe(2)-Fe(1)-S(3) 53.77(2), Fe(2)-Fe(1)-P(1) 117.45(2), Fe (2)-Fe(1)-P(2) 119.51(2), Fe(2)- *S*(1)-Fe(1) 71.73(2) Fe(2)- *S*(3)-Fe(1) 71.82(2), Fe(2)-Fe(1)-C(1) 102.47 (6), Fe(2)-Fe(1)-C(2) 142.67(6).

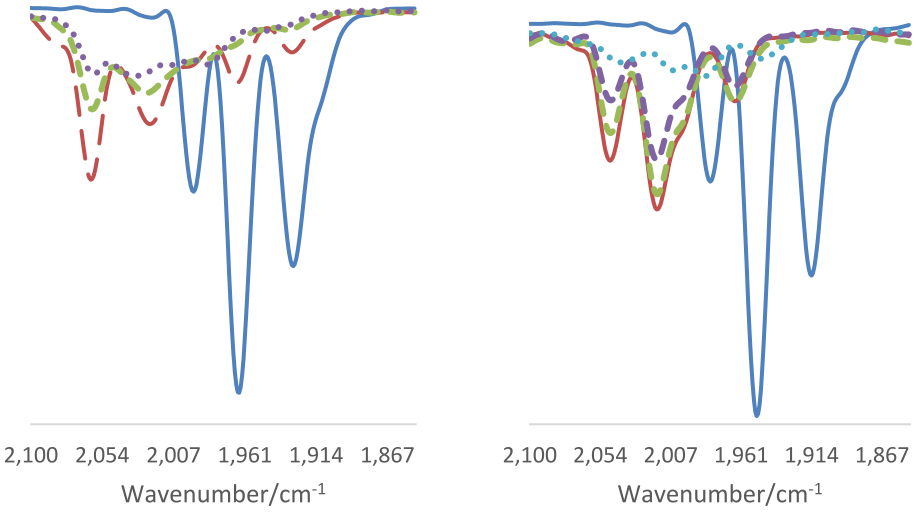

a **b**

Fig. 6. (a) Infra-red spectra of $[Fe_2(CO)_4(\mu\text{-sdt})(\mu\text{-dppm})]$ (**2**) in CH_2Cl_2 (transmittance mode) – blue (Complex **2**), red (Complex **2** + HBF_4 after 30 s), green (Complex **2** + HBF_4 after 15 min), and purple (Complex **2** + HBF_4 after 40 min); (b) FTIR spectra of $[Fe_2(CO)_4(\mu\text{-sdt})(\mu\text{-dcpm})]$ (**3**) in CH_2Cl_2 blue (Complex **3**), red (Complex **3** + HBF_4 after 1 min), green (Complex **3** + HBF_4 after 45 min), purple (Complex **3** + HBF4 after 2 h 30 min), and light blue (Complex **2** + HBF_4 after 14 h 30 min).

Table 1
Measured redox potentials for complexes **1**–**9**.

Compound in MeCN solution	$E_{red}(V)$	$E_{red}(V)$	$E_{ox}(V)$	$E_{ox}(V)$
$[Fe_2(CO)_6(\mu\text{-SCH})_2S]$ (**1**)[20]		−1.50		
$[Fe_2(CO)_4(\mu\text{-sdt})(\mu\text{-dppm})]$ (**2**)	−2.13	−1.96		0.42
$[Fe_2(CO)_4(\mu\text{-sdt})(\mu\text{-dcpm})]$ (**3**)	−2.33	−2.11	0.18	
$[Fe_2(CO)_4(\mu\text{-sdt})(\mu\text{-dppf})]$ (**8**)	−2.44	−1.93	0.08	
$[Fe_2(CO)_4(\mu\text{-sdt})(k^2\text{-dppv})]$ (**4**)	−2.16	−1.93	NR	NR
$[\{Fe_2(CO)_4(\mu\text{-sdt})\}_2(\mu\text{-}k^1,k^1\text{-dppe})]$ (**5**)	−2.06	−1.70		0.48
$[Fe_2(CO)_4(\mu\text{-sdt})(k^1\text{-dppfO})]$ (**6**)	−2.14	−1.71	0.29	0.47
$[\{Fe_2(CO)_4(\mu\text{-sdt})\}_2(\mu\text{-}k^1,k^1\text{-dppf})]$ (**7**)	−2.02	−1.76	0.24	NR
$[Fe_2(CO)_5(\mu\text{-sdt})(PPh_3)]$ (**9**)	−1.93	−1.70	0.09	0.45

(s), 2040(s), 2001(s) cm^{-1}) by the diphosphines, consistent with the buildup of electron density on the iron centers in the $Fe_2(CO)_x$ core, in line with observations made for analogous complexes with related bridging dithiolate ligands [30,31].

The ^1H NMR spectrum of the complexes contain resonances of the methylene moieties from sdt ligands in addition to the phenyl proton resonances in the aromatic region. The constraint of the single methylene moiety in between the two phosphines appears to prevent the dppm and dcpm ligand from coordinating in a chelating coordination mode, which would lead to the formation of four-membered Fe-P-C-P rings [31]. The $^{31}P\{^1H\}$ NMR spectra display singlets at $\delta = 52.9$, 60.0, 51.0 for **2**, **3**, and **8**, respectively, which indicate that the two phosphines of the diphosphine ligand are in chemically and magnetically equivalent positions [30].

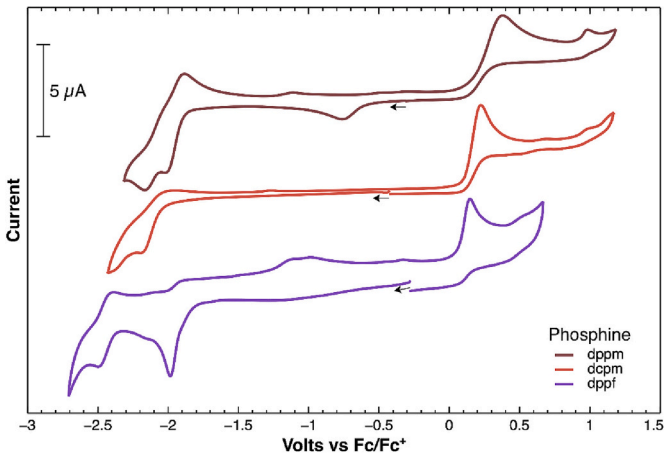

Fig. 7. CVs of **2** (dppm), **3** (dcpm) and **8** (dppf) in MeCN (1 mM solution, supporting electrolyte $[NBu_4][PF_6]$ at 100 mV/s scan rate, glassy carbon electrode (gce), potential vs Fc^+/Fc).

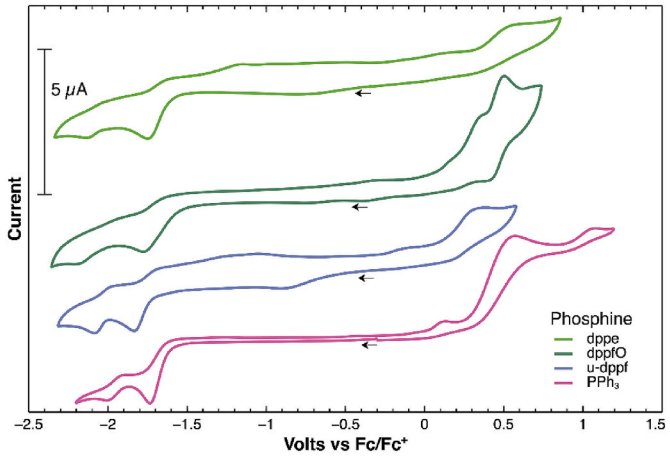

Fig. 8. Cyclic voltammograms of **5**, **6**, **7** and **9** (PPh_3) in MeCN (1 mM solution, supporting electrolyte $[NBu_4][PF_6]$ at 100 mV/s scan rate, glassy carbon electrode (gce), potential vs Fc^+/Fc).

3.3.2. *Chelating coordination of dppv*

Complex **1** was treated with dppv, producing $[Fe(CO)_4(\mu\text{-sdt})(\kappa^2\text{-dppv})]$ (**4**), in which the diphosphine ligand chelates to one iron in the complex. The *cis* geometry of the backbone in dppv predisposes the ligand to a chelating coordination mode and makes an intramolecular bridging coordination mode less favored because of the geometric rigidity of the ligand. The FTIR absorptions in the carbonyl region for complex **4** are characteristic of $[Fe_2(CO)_4(\mu\text{-sdt})(\kappa^2\text{-diphosphine})]$ and $[Fe_2(CO)_4(\mu\text{-adt})(\kappa^2\text{-diphosphine})]$complexes [30,36,37]; they are found at 2022(s), 1949(s), and 1918(sh) cm^{-1}. Analysis by ^1H NMR is uninformative, showing resonances attributed to the ethylene protons of the dppv ligand in addition to other proton resonances. The $^{31}P\{^1H\}$ NMR spectrum of the complex indicates that it exists in two isomeric forms in solution due to a trigonal twist of the $Fe(CO)(\kappa^2\text{-dppv})$ unit that is commonly observed in complexes of this kind [31–33]. The $^{31}P\{^1H\}$ NMR spectrum of complex **4** displays a singlet at $\delta = 83$ ppm together with a smaller singlet at $\delta = 76$ ppm that are ascribed to the basal-apical and dibasal isomers (Fig. 2). Such isomerism has been previously observed in complexes of this type with exchange between isomers occurring on the NMR timescale [32].

3.3.3. *Intermolecular bridging coordination of diphosphines*

A bridging intermolecular coordination of two diiron clusters was identified by treatment of **1** with dppe, producing $[\{Fe_2(CO)_4(\mu\text{-sdt})\}_2(\mu\text{-}\kappa^1;\kappa^1\text{-dppe})]$ (**5**). The increased flexibility due to the presence of an extra methylene group in the backbone, relative to dppm, facilitates the coordination of dppe to a second diiron unit. The spectroscopic features of **5** resemble those of reported and structurally characterized tetra-iron complexes of the general formula $[\{(\mu\text{-edt})Fe_2(CO)_5\}_2(\mu\text{-L})]$ (L = diphosphine) [34]. The FTIR spectrum of **5** shows a $\nu_{(C-O)}$ pattern with two strong resonances at 2048 and 1986 cm^{-1}, a medium shoulder at 1963 cm^{-1}, and a small absorption at 1933 cm^{-1}, which closely resembles those of previously reported related tetrairon (dimer of dimer) compounds [30,34]. The ^1H NMR spectrum shows two singlets at $\delta =$ 2.8 ppm and 2.1 ppm for the methylene moieties in the sdt ligand and dppe, respectively. In the ^{31}P NMR spectrum of **5**, a singlet at $\delta = 58.8$ ppm was found, in agreement with two phosphorus atoms in chemically and magnetically equivalent environments [34].

The ligand 1,1′-bis(diphenylphosphino)ferrocene (dppf), provides an additional iron ion that, in principle, can be involved in electron transfer and proton reduction. The identity of $[\{Fe_2(CO)_4(\mu\text{-sdt})\}_2(\mu\text{-}\kappa^1;\kappa^1\text{-dppf})]$ (**7**), which contains dppf spanning two diiron clusters with each phosphine moiety coordinating in monodentate fashion to one diiron unit, was confirmed by a comparison of its physicochemical data to those previously published by Song et al. [41] (cf. Table S1, Supplementary Material).

3.3.4. *Monodentate coordination of phosphines*

The reaction of **1** with dppf also yielded a second product that was identified as $[Fe_2(CO)_4(\mu\text{-sdt})(\kappa^1\text{-dppfO})]$ (**6**), containing a partially oxidized diphosphine. Such a partially oxidized dppf ligand has been observed previously when $[Fe_2(CO)_6(\mu\text{-toluene-3,4-benzenedithiolate})]$ was reacted with dppf to yield three products, one of which contains oxidized dppf [39]. The source of the oxygen atom is unknown; it may originate from trimethyl amine N-oxide or adventitious water. Two peaks were found in the ^{31}P NMR spectrum: the first peak at 40.7 ppm is attributed to the coordinated phosphine of the dppf ligand while the second peak at 28.2 ppm is attributed to the non-coordinated oxidized phosphine unit. The free dppf ligand has a negative ^{31}P NMR shift value, indicating that the "dangling" phosphine moiety does not correspond to the normal, unoxidized ligand.

In addition, the known monodentate triphenylphosphine derivative of **1**, $[Fe_2(CO)_5(\mu\text{-sdt})(\kappa^1\text{-}PPh_3)]$ (**9**), was prepared and identified in accordance with the published synthetic procedure and physicochemical data [41].

3.4. *Structural studies*

The molecular structures of **2**, **3** and **8** are depicted in Figs. 3–5. Relevant crystallographic data are summarized in Table S2, and full lists of bond distances and bond angles are found in Tables S3–S9 (Supplementary Material). Each of the solid-state structures of **2**, **3**, and **8** contain a diiron framework bridged by a sulfurdithiolato and a diphosphine ligand (dppm, dcpm, dppf) in addition to the terminal carbonyls that complete the coordination spheres of the metals. Disregarding the iron-iron bond, each iron possesses a slightly distorted square pyramidal coordination geometry.

The crystal structure of $[Fe_2(CO)_4(\mu\text{-sdt})(\mu\text{-dppm})]$ (**2**) is depicted in Fig. 3 with the caption containing selected bond distances and angles. The molecule is similar to analogous complexes that have a butterfly [2Fe2S] cluster core whose two iron atoms are bridged by a diphosphine ligand with a symmetrical chelate *cisoid* basal-basal coordination pattern, four terminally coordinated carbonyls and a sulfurdithiolate ligand that is linked to the two irons. Each iron core adopts a slightly distorted square-pyramidal geometry. Complex **2** has a slightly shorter Fe—Fe bond distance Fe(1)-Fe(2) 2.50508(4) Å than the parent compound **1** (Fe—Fe 2.5120(5) Å) [20]), and shorter than the Fe—Fe distance for the pdt analogue (2.5479 Å) [38]. The Fe—S bond distances in **2** are very similar to those observed for **1** [20] and other analogous

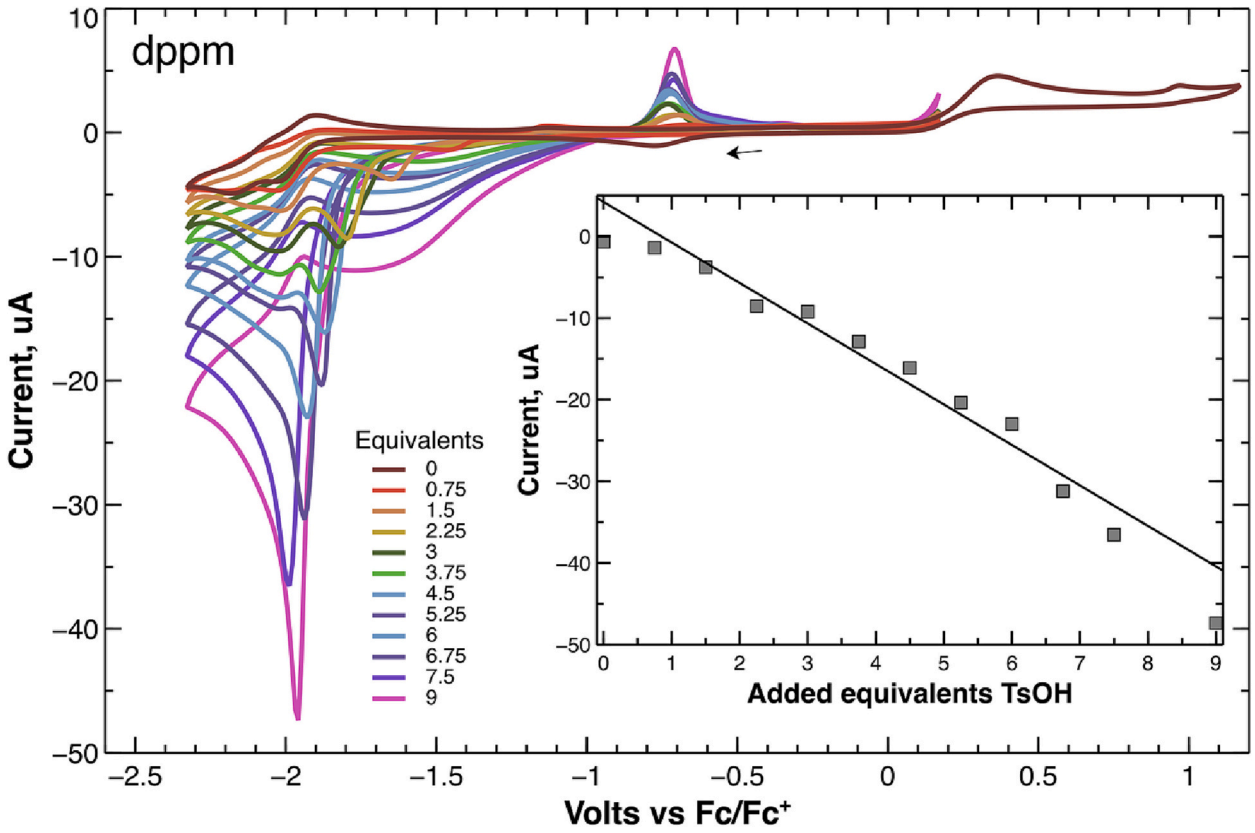

Fig. 9. Cyclic voltammograms of $[Fe_2(CO)_4(\mu\text{-sdt})(\mu\text{-dppm})]$ (**2**) in the presence of 0–9 M equivalents of *p*-TsOH (1 mM solution in MeCN, supporting electrolyte $[NBu_4][PF_6]$, scan rate 0.1 Vs^{-1}, glassy carbon electrode, potential vs. Fc^+/Fc). Current values have been corrected for dilution. The inset shows the proton reduction peak current.

dithiolate complexes. The Fe—P bond distances of 2.2553(7) and 2.2179 (6) Å in **2** are within the range reported for related diiron-dithiolates complexes.

The solid-state molecular structure of $[Fe_2(CO)_4(\mu\text{-sdt})(\mu\text{-dcpm})]$ (**3**) is depicted in Fig. 4. The molecule contains a diiron core, a coordinated dcpm ligand and a bridging sulfur dithiolate ligand. The Fe—Fe bond distance of 2.531(2) in complex **3** is slightly longer than that of the parent complex **1** (Fe—Fe 2.5120(5)) Å [20] and compares well with the Fe—Fe bond distance 2.5259(10) Å found in $[Fe_2(CO)_4(\mu\text{-dcpm})(\mu\text{-pdt})]$ [42]. The Fe—S bond distances of **3**, 2.256(2) and 2.252(2) Å, are very similar to those observed for **1** at 2.2514(5) Å [20] and the pdt analogue at 2.2701(14) Å [42]. The dcpm ligand of **3** binds to the diiron core in a *cisoid* dibasal fashion with an Fe—P bond distance of Fe(1)-P(1) 2.245(2) Å, which is almost identical to that of the pdt analogue at 2.248(1) Å [42]. The cyclohexyl moieties of the dcpm ligand are stabilized in the chair conformation.

The molecular structure of $[Fe_2(CO)_4(\mu\text{-sdt})(\mu\text{-dppf})]$ (**8**) is depicted in Fig. 5. The structure of complex **8** is similar to those of complexes **2** and **3**, containing a diiron core ligated by four carbonyls, a dppf, and a bridging sulfur dithiolato ligand. The molecule has expected bond lengths and angles which is generally within the ranges of those seen in related complexes [31,34,35]. The Fe—Fe bond length is Fe(1)-Fe(2) 2.6402(6) in complex **8**, which is a bit longer than in the pdt analogue (Fe(1)–Fe(2) 2.6133(6)), complex **2** (Fe(1)-Fe(2) 2.5058(4)), and **3** (Fe (1)-Fe(2) 2.5318(2)).

3.5. Reaction with Brönsted and Lewis acids

In order to be able to determine or propose a catalytic mechanism for proton reduction effected by the metal complexes, it is important to know where protons can bind in the diiron dithiolate complexes. In the present study, there are two likely sites for protonation – the metal ions and/or the sulfur in the bridge head. Hogarth and coworkers, and other groups, have reported that diiron tetracarbonyl complexes with bidentate phosphine ligands are directly protonated at the Fe—Fe bond to form a stable hydride [42–47]. As mentioned in the introduction, phosphine substitution affects the Lewis basicity of the diiron core and may thus also affect the protonation behavior. A qualitative assessment of the protonation behavior can be obtained by introducing a strong acid to a solution of the complex and monitoring its IR spectrum in the carbonyl region. The addition of one equivalent or excess amounts of HBF_4Et_2O to CH_2Cl_2 solutions of the diiron complexes is expected to generate sufficient Brönsted acidity for the compounds to be protonated at room temperature.

Protonation of the diphosphine-bridged complexes **2**, **3** and **8** with HBF_4Et_2O or *p*-TsOH was studied through *in situ* IR spectroscopy as depicted in Fig. 6. For these three neutral complexes, the IR spectra show three carbonyl absorption bands at 1994, 1965, and 1929 cm^{-1}; 1981, 1950, and 1914 cm^{-1}; and 1991, 1957, and 1924 cm^{-1}, respectively. Upon the addition of one equivalent of HBF_4Et_2O, the observed carbonyl stretching frequencies of **2** and **3** in the IR spectra shifted gradually in positive direction. New absorption peaks appeared at 2059, 2025, and 1984 cm^{-1} for **2**, and 2047, 2017, and 1955 cm^{-1} for **3**, a shift by ca. 40–70 wavenumbers to higher values, as depicted in Fig. 6. The shifts suggest metal-centered protonation, presumably resulting in the clean formation of the cationic hydrides $[Fe_2(CO)_4(\mu\text{-sdt})(\mu\text{-H})(\mu\text{-dppm})][BF_4]$ (**2H**) and $[Fe_2(CO)_4(\mu\text{-sdt})(\mu\text{-H})(\mu\text{-dcpm})][BF_4]$ (**3H**). These protonated species are stable and after 14 h the shifted absorptions at 2050, 2031, and 1984 for **2** and at 2040, 1984, and 1947 cm^{-1} for **3**, can still be discerned although the intensities are significantly reduced, presumably due to decomposition. For complex **8**, the IR spectrum shows resonances at 1991, 1957, and 1924 cm^{-1}, as depicted in Fig. S1

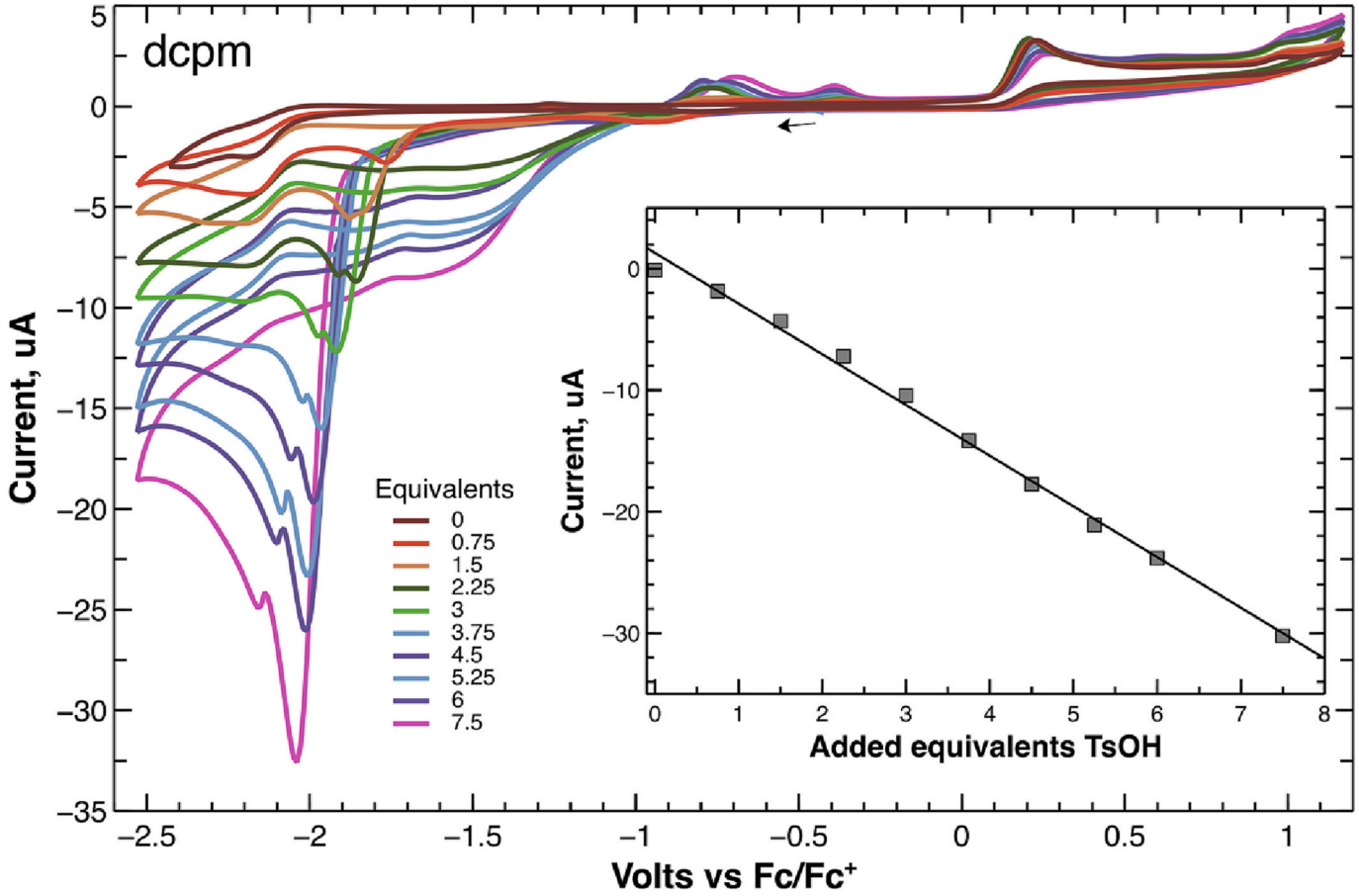

Fig. 10. Cyclic voltammograms of $[Fe_2(CO)_4(\mu\text{-sdt})(\mu\text{-dcpm})]$ (**3**), in the presence of 0–7.5 M equivalents of *p*-TsOH (1 mM solution in MeCN, supporting electrolyte $[NBu_4][PF_6]$, scan rate 0.1 Vs^{-1}, glassy carbon electrode, potential vs. Fc^+/Fc). Current values have been corrected for dilution. The inset shows the proton reduction peak current.

(Supplementary Material). There are no shifts of the peaks upon addition of HBF_4Et_2O, even after 16 h, suggesting that a stronger acid may be needed to achieve protonation, or that protonation is very slow.

Upon addition of excess acid to the chelate complex **4**, the IR spectrum shifts from 2020, 1950, and 1919 cm^{-1} to 2115, 2040 and 1980 cm^{-1}, resulting in a large shift by approximately 90 wavenumbers as depicted in Fig. S2 (Supplementary Material). The new IR spectrum may be ascribed to the metal protonated species $[Fe_2(CO)_4(\mu\text{-sdt})(\mu\text{-H})(\kappa^2\text{-dppv})]$ (**4H**). This is in accordance with previously reported results on reaction of chelated diiron dithiolate diphosphine analogues with HBF_4Et_2O that found that the protonation occurs at the metal center [43,47–54]. Compound **4H** was found to be unstable and all absorption intensities were reduced after 30 min. For **5**, the neutral complex shows absorptions at 2050, 1967, and 1934 cm^{-1}, as depicted in Fig. S3 (Supplementary Material). There are no shifts of these peaks upon addition of acid even after 16 h, suggesting that complex **5** is not sufficiently basic to be protonated under the conditions used and that a stronger acid needs to be used. The IR absorptions of **5** were found to gradually decrease over time and a change in the color of the solution occurs, implying a partial decomposition. Infrared measurements on the mono-substituted complex $[Fe_2(CO)_5(\mu\text{-sdt})(PPh_3)]$ (**9**) [41] showed only partial protonation by excess $HBF_4{\cdot}Et_2O$. The protonation led to a shift of the $\nu_{(C\text{-}O)}$ resonances to higher wavenumbers, with new resonances appearing at 2121w, 2105w, 2086w, 2062 m within 10 min (Fig. S4). The resonances were thus shifted by 50–100 cm^{-1}, in agreement with protonation at the metal center.

Attempts to monitor the protonation of the diiron complexes via ^1H NMR were unsuccessful because of the very large signal from free acid leading to significant difficulties in resolving any other resonances.

3.6. Electrochemistry

Weigand and co-workers investigated the electrochemical properties of $[Fe_2(CO)_6(\mu\text{-sdt})]$ (**1**) and found that a two-electron reduction proceeds in a stepwise manner [20]. The effect on the electrochemical properties of substituting carbonyl ligands of **1** with phosphines was ascertained by performing cyclic voltammetry on **2**–**9** in CH_3CN under nitrogen atmosphere. The observed redox potentials for the complexes are listed in Table 1. The diphosphine-bridged complexes show similar behavior with two quasi-reversible reductions. The redox behaviors of **2**, **3** and **8** (Fig. 7) are similar with reductions at −1.96, −2.11, and − 1.93, another reduction at −2.13, −2.33, and − 2.44, and an oxidation at 0.42, 0.18, 0.08 *V*, respectively. The cyclic voltammetry of diirondithiolate complexes containing intramolecularly bridging diphosphines have been shown to exhibit a lack of reversibility in both oxidation and reduction steps in CH_3CN [31,52,53]. For example, Hogarth and co-workers reported electrochemical redox behavior for the related bridging complex $[Fe_2(CO)_4\{\mu\text{-}Ph_2PN(R)PPh_2\}(\mu\text{-pdt})]$ (R = allyl), which shows similar oxidation and reduction behavior to complexes **3** and **8** [31]. The Fe(II)/Fe(III) couple for the iron ion of the dppf ligand is not reversible. Differential pulse voltammetry confirms that it occurs at +0.08 *V* vs Fc^+/Fc (Fig. S6). The chelating complex **4** exhibits two quasi-reversible reductions at ca. −1.93 and − 2.16 V and electrochemical properties similar to those observed for $[Fe_2(CO)_4(\kappa_2\text{-dppe})\{\mu\text{-}SCH_2N(R)CH_2S\}]$ (R) = iPr, CH_2CH_2OMe and $CH_2C_6H_5$) (Fig. S7, Supplementary Material) [53].

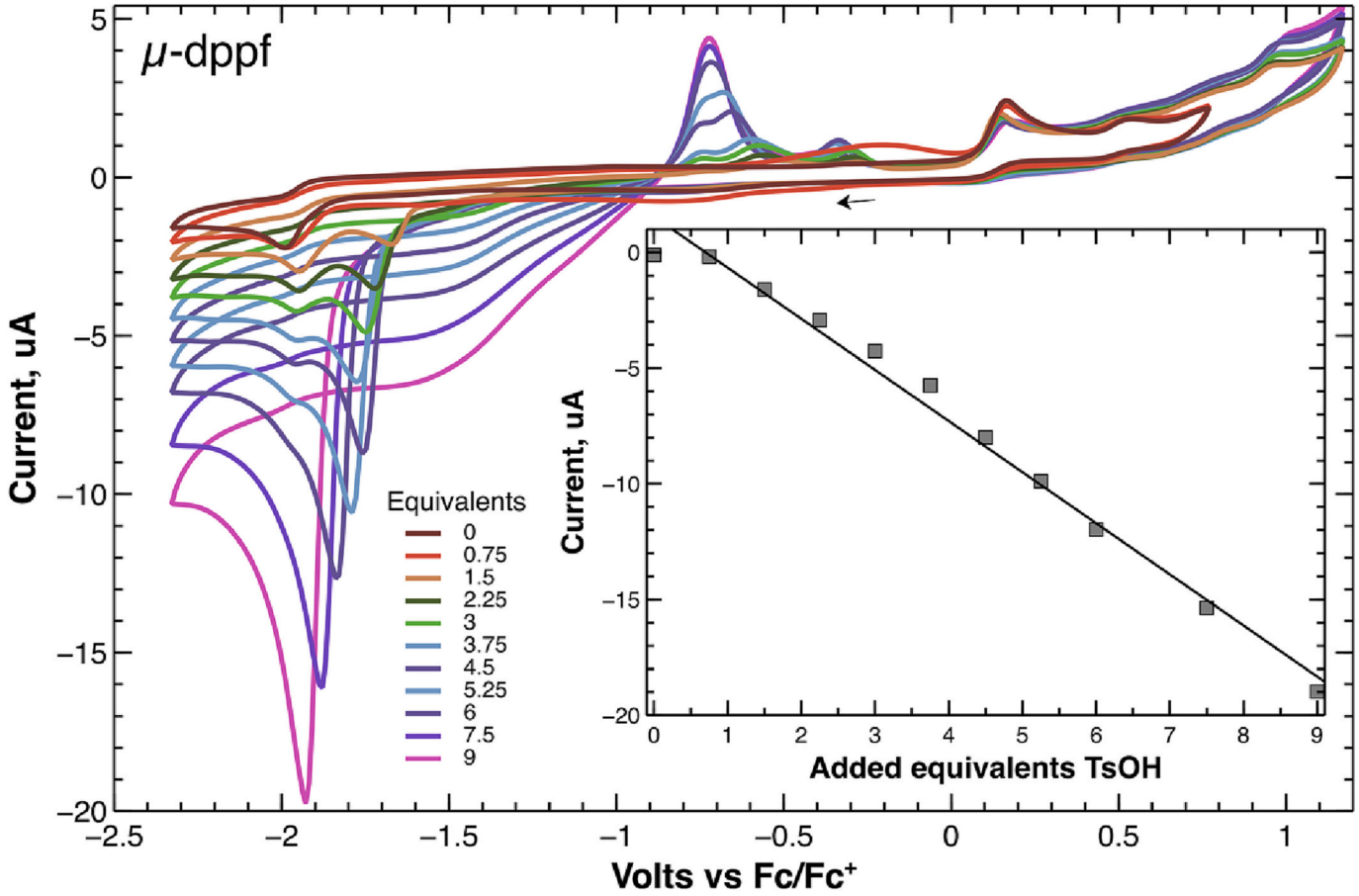

Fig. 11. Cyclic voltammograms of $[Fe_2(CO)_4(\mu\text{-sdt})(\mu\text{-dppf})]$ (**8**) in the presence of 0–9 M equivalents of *p*-TsOH (1 mM solution in MeCN, supporting electrolyte $[NBu_4][PF_6]$, scan rate 0.1 Vs^{-1}, glassy carbon electrode, potential vs. Fc^+/Fc). Current values have been corrected for dilution. The inset shows the proton reduction peak current.

The intermolecularly bridged tetranuclear mono-substituted complexes **5** and **7**, and the mono-substituted complexes **6** and **9**, show similar electrochemical properties (Fig. 8). They are more easily reduced with quasi-reversible reduction peaks at ca. −1.70, −1.71, −1.76 and −1.70 *V*, followed by a smaller reduction at −2.06, −2.14, −2.02 and −1.93 V for **5**, **6, 7** and **9**, respectively. Oxidation peaks were observed at 0.48, 0.29, 0.24 and 0.09 V for **5**, **6, 7** and **9**, and an additional oxidation was observed at 0.47 and 0.45 V for **6** and **9**. The mono-substituted complexes **6** and **9** shows similar behavior with the reported complex $[\{Fe_2(CO)_5(\mu\text{-(pdt)}\}_2(PPh_3)]$ in which the bridging propane dithiolate (pdt) ligand acts as a monodentate phosphine ligand to two diiron units [40]. Åkermark and co-workers reported that two butterfly complexes where two Fe_2S_2 units are linked by the diphosphine ligand showed a reduction at −1.93 *V* and an oxidation at 0.62 V for $[\{Fe_2(CO)_5(\mu\text{-}(SCH_2)_2N(ethyl))\}_2(\mu\text{-}\kappa^1\text{-}\kappa^1\text{-dppe})]$ and a reduction at −1.94 V and oxidation at 0.67 V for $[\{Fe_2(CO)_5(\mu\text{-(pdt)}\}_2(\mu\text{-}\kappa^1\text{-}\kappa^1\text{-dppe})]$ in CH_2Cl_2 [54], which are close to the potentials found for complex **5**.

In the cyclic voltammograms of all complexes, it was found that the first reduction potential is shifted ca. 0.3 V to more negative potentials for the diphosphine-substituted complexes relative to the mono-substituted complexes; an indication of greater electron density on the diiron centers of the former kind of complexes due to the presence of more coordinating phosphine entities. This is in agreement with observations made for related phosphine-substituted complexes [55].

3.7. Electrocatalytic studies

Electrocatalytic proton reduction studies were carried out on **2**–**5**, **8** and **9** in the presence of *para*-toluene sulfonic acid (*p*-TsOH) in CH_3CN and in each case a catalytic response was observed. The results of these studies are displayed in Figs. 9–13 and Figs. S8–S14 (Supplementary Material). As discussed above, protonation experiments on complexes **2** and **3** in the presence of 2–3 equivalents of *p*-TsOH or HBF_4Et_2O in CH_2Cl_2 show the evidence of protonation at the metal core (Fig. 6). Addition of two equivalents of *p*-TsOH to **2**, **3** and **8** leads to the appearance of new irreversible catalytic reduction peaks at −1.7 for **2**, −1.8 V for **3**, and − 1.7 V for **8**, respectively (Figs. 9–11 and S8–S10). The protonation and electrocatalysis studies suggest the formation of the cationic hydride complexes $[Fe_2(CO)_4(\mu\text{-sdt})(\mu\text{-H})(\mu\text{-dppm})]$ (**2H**$^+$), $[Fe_2(CO)_4(\mu\text{-sdt})(\mu\text{-H})(\mu\text{-dcpm})]$ (**3H**$^+$) and $[Fe_2(CO)_4(\mu\text{-sdt})(\mu\text{-H})(\mu\text{-dppf})]$ (**8H**$^+$). The height of the new peaks increase with increasing acid concentration (see Figure insets). This behavior is characteristic of electrocatalytic proton reduction by the complexes, and presumably involves the intermediate formation of the above-mentioned hydrides. While evidence for protonation of **8** by HBF_4 could not be obtained (see above), its electrocatalytic behavior suggests that **8** is protonated in the presence of *p*-TsOH. Upon increasing acid concentration, the peak shifts to more negative potentials for complexes **2, 3** and **8** (Figs. 9–11 and S8–S10).

These complexes may be entering into the catalytic process via a chemical step (protonation) which could be followed by an electrochemical reduction to generate the neutral 35-electron complexes **2(μ-H)**, **3(μ-H)** and **8(μ-H)**. These neutral complexes can be either protonated or undergo a further reduction before a second protonation for liberation of molecular hydrogen. All the C*V*s have the common character trait that they show curve-crossing at multiple equivalents of

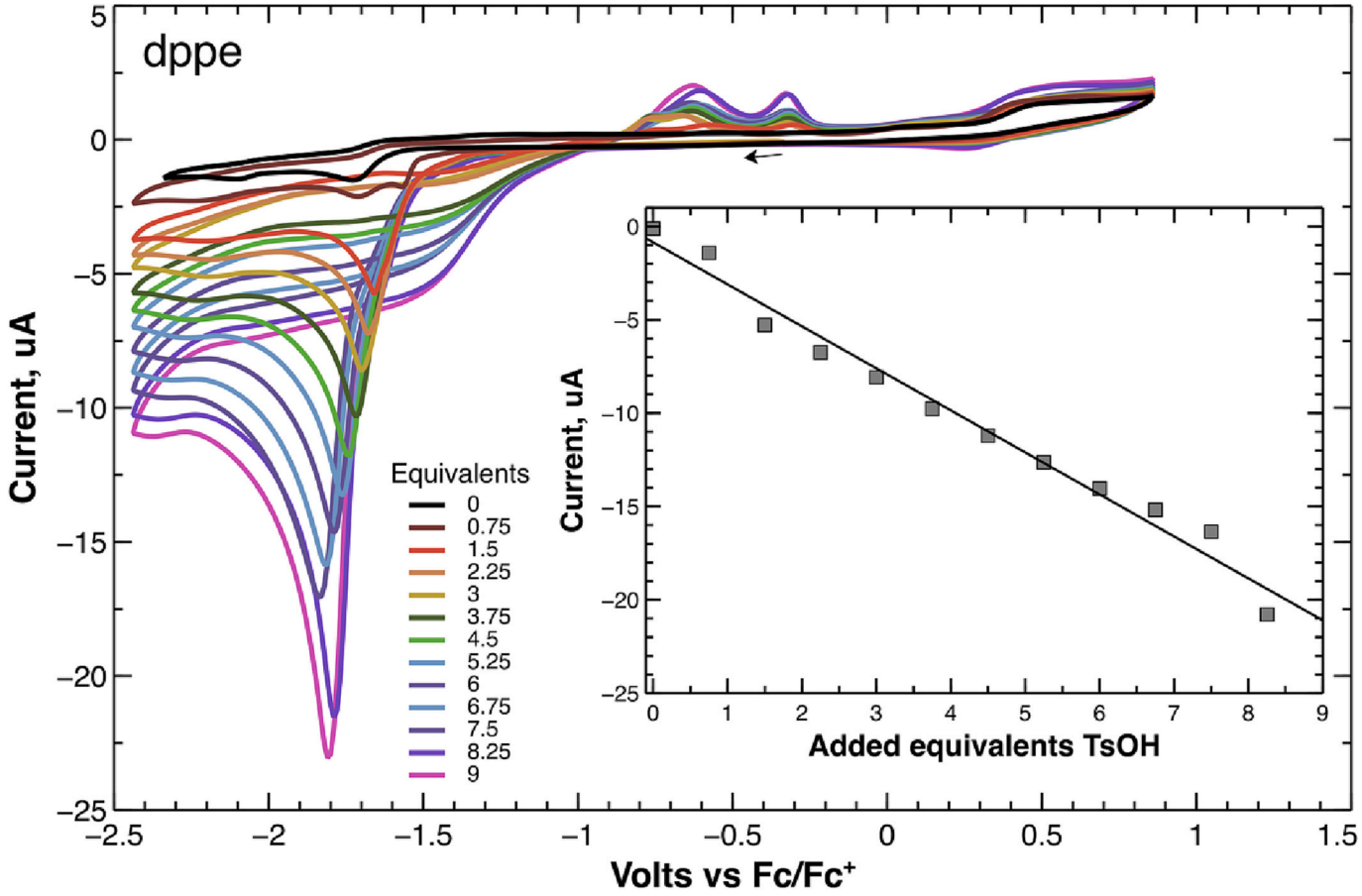

Fig. 12. Cyclic voltammograms of [{$Fe_2(CO)_5$(μ-sdt)}$_2$(μ-κ^1-κ^1-dppe)] (**5**) in the presence of 0–9 M equivalents of *p*-TsOH (1 mM solution in MeCN, supporting electrolyte [NBu_4][PF_6], scan rate 0.1 Vs^{-1}, glassy carbon electrode, potential vs. Fc^+/Fc). Current values have been corrected for dilution. The inset shows the proton reduction peak current.

TsOH, i.e., a build-up of reduction current on the return scans at ca. −1.8 V during the catalytic cycles. This feature suggests that an easily reducible intermediate is formed during the catalysis, possibly via a slow chemical reaction. This product is relatively stable and increases with increasing acid concentration, and it diffuses back to the electrode to undergo reduction at more positive potential. This electrochemical behavior has been observed for a number of related diiron dithiolate complexes [56–66].

The protonation experiment on complex **4** in the presence of 2–3 equivalents of *p*-TsOH or HBF_4Et_2O in CH_2Cl_2 show an appearance of new IR peaks toward higher wavenumbers. This observation indicates that the complex is protonated, but unfortunately the protonated species is not stable in the acidic medium (Fig. S2). Voltammetry catalytic studies on complex **4** (Fig. S8) show a new catalytic reduction peak at −1.5 V, which is more positive than the reduction potential of free *p*-TsOH, and the height of the reduction wave increases with the addition of successive molar equivalents of *p*-TsOH. Complex **4** was not studied further since the complex lacks stability in the acidic medium.

For the mono-substituted complex **5**, the catalytic reduction peak observed at −1.7 *V* does not shift toward more positive potentials with added acid (Fig. 12 and S11). In the protonation studies discussed above, complex **5** did not show any evidence of protonation. In the presence of 2–3 equivalents of *p*-TsOH or HBF_4Et_2O in CH_2Cl_2, no change in the IR spectrum of **5** was detected (Fig. S3). The height of the reduction wave increases with the addition of successive molar equivalents of *p*-TsOH, indicating that **5** catalyzes proton reduction at its first reduction potential.

Although IR spectroscopy indicated only partial protonation of the mono-substituted complex [$Fe_2(CO)_5$(μ-sdt)(PPh_3)] (**9**), the complex exhibited good catalytic proton reduction activity in the presence of excess *p*-TsOH (Figs. 13 and S12). In addition, complex **9** effects proton reduction at a potential that is more positive than that which occurs for free *p*-TsOH (Fig. S13). The small oxidation waves around −0.7 V that are shown in Figs. 9–13 are only observed in the presence of TsOH and after scanning through the irreversible peak near −2.0 V. It is likely that the oxidation comes from an unidentified side product produced by partial decomposition of the reduced species.

4. Summary and conclusion

In this study, we have probed the electron density of the metal core of a number of diiron carbonyl complexes by exchanging carbonyl ligands with a number of diphosphine ligands, and we have studied how this ligand substitution affects the proton reduction ability of the complexes. Several new diiron complexes have been synthesized in moderate yields: [$Fe_2(CO)_4$(μ-sdt)(μ-dppm)] (**2**), [$Fe_2(CO)_4$(μ-sdt)(μ-dcpm)] (**3**), [$Fe_2(CO)_4$(μ-sdt)(κ^2-dppv)] (**4**), [{$Fe_2(CO)_5$(μ-sdt)}$_2$(μ-κ^1-κ^1-dppe)] (**5**), [$Fe_2(CO)_5$(μ-sdt)(κ^1-dppfO)] (**6**), [{$Fe_2(CO)_5$(μ-sdt)}$_2$(μ-κ^1-κ^1-dppf)] (**7**), [$Fe_2(CO)_4$(μ-sdt)(μ-dppf)] (**8**), and [$Fe_2(CO)_5$(μ-sdt)(κ^1-PPh_3)] (**9**). Single crystal analysis of complexes **2**, **3**, and **8** revealed that each of these clusters possesses a butterfly Fe_2S_2 core with the sulfur dithiolato ligand coordinated to the diiron metal center, a bridging diphosphine in a basal-basal position, and four terminal carbonyls completing the ligand environment, while **9** possesses a monodentate phosphine coordinated in an apical position. In protonation studies, IR spectroscopy shows that complexes **2** and **3** are protonated at the metal core, while complexes **5**, **6**, and **7** are inert when acidified by HBF_4Et_2O. Complex **4**, in which the diphosphine coordinates in a chelating mode, and

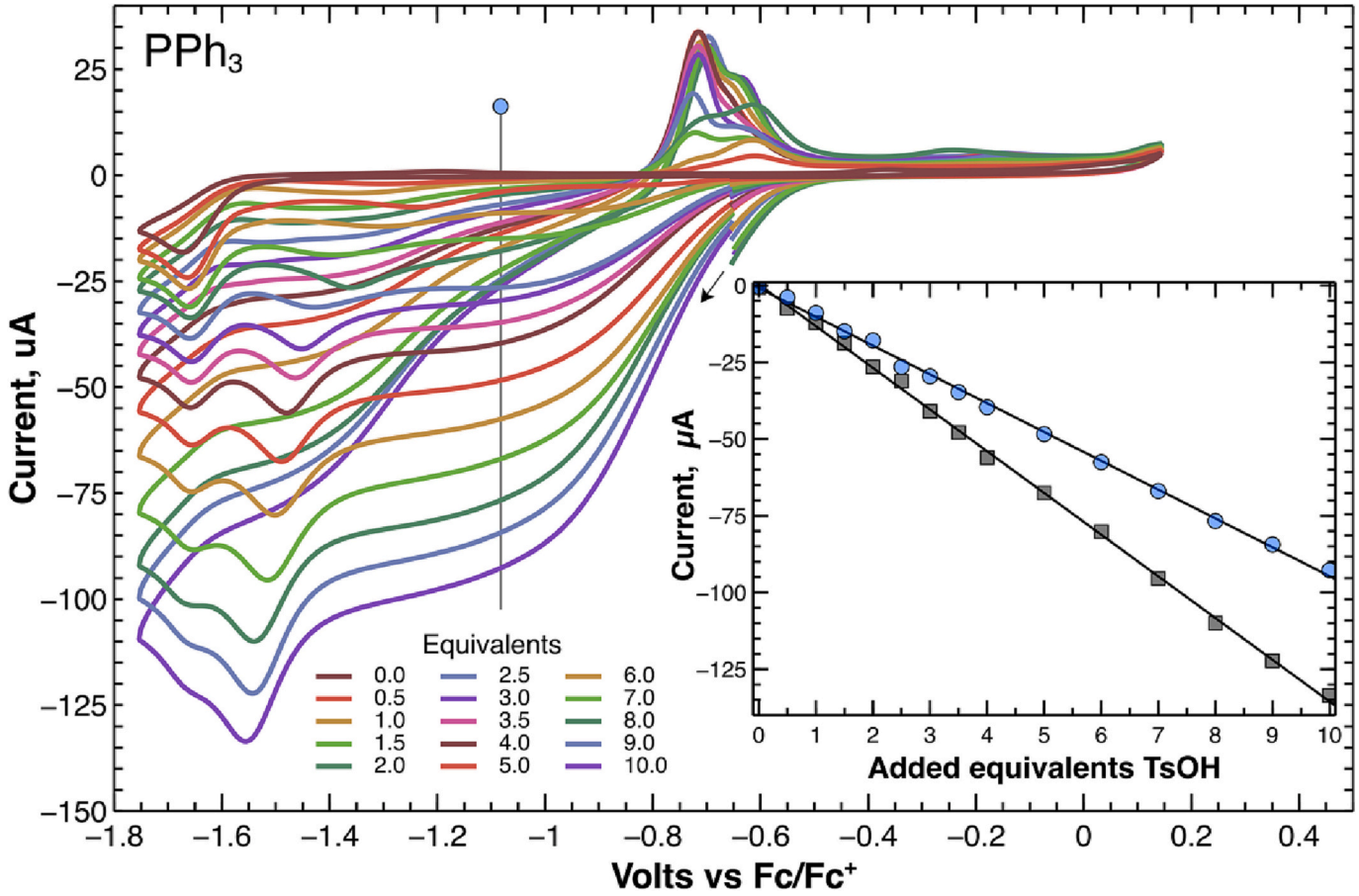

Fig. 13. Cyclic voltammograms of $[Fe_2(CO)_5(\mu\text{-sdt})(\kappa^1\text{-}PPh_3)]$ (**9**) in the presence of 0–10 M equivalents of *p*-TsOH (1 mM solution in MeCN, supporting electrolyte $[NBu_4][PF_6]$, scan rate 0.1 Vs^{-1}, 3 mm platinum electrode, potential vs. Fc^+/Fc). Current values have been corrected for dilution. The inset shows the proton reduction peak current as well as the current at −1.08 V vs. Fc^+/Fc.

complexes **2**, **3**, and **8** possess diiron cores that are sufficiently basic to be protonated. The basicity of these complexes is due to the fact that two carbonyl ligands are replaced by phosphine moieties of the specific diphosphine ligand, leading to higher electron density on the metal core. On the other hand, complexes **5**, **6**, **7** and **9** tend to be more stable and not sufficiently basic to be fully protonated because in these complexes only one carbonyl ligand of each diiron core is replaced by a phosphine moiety of the diphosphine ligand. The increased electron density on the metal cores in all diphosphine complexes, relative to the parent cluster $[Fe_2(CO)_6(\mu\text{-sdt})]$ (**1**), is reflected in their redox chemistry and electrocatalysis. In comparison to the parent compound **1**, which has a reduction peak −1.5 *V* that is shifted to −1.55 V upon addition of acid and resultant electrocatalytic proton reduction, complexes **2–8** display reduction waves at more negative potentials (in the range −1.7 to −2.1 V). Thus, while diphosphine substitution at the diiron core leads to increased electron density at the diiron core and facilitates protonation at the metal centers, a price is paid in the respect that proton reduction catalysis is shifted to more negative potentials relative to the unsubstituted metal core. On the other hand, monosubstituted **9** displays efficient electrocatalysis at relatively low overpotentials.

CRediT authorship contribution statement

Lintang Hizbullah: Investigation, Methodology, Writing – original draft, Writing – review & editing. **Ahibur Rahaman:** Conceptualization, Investigation, Methodology, Writing – original draft, Writing – review & editing. **Seyedeh Safavi:** Investigation. **Matti Haukka:** Investigation, Validation, Writing – review & editing. **Derek A. Tocher:** Investigation, Validation. **George C. Lisensky:** Investigation, Methodology, Writing – original draft, Writing – review & editing. **Ebbe Nordlander:** Conceptualization, Supervision, Project administration, Funding acquisition, Writing – review & editing.

Declaration of Competing Interest

There are no competing interests to declare.

Data availability

Data will be made available on request.

Acknowledgements

This paper is dedicated to the memory of Professor Ademir Neves, a pioneer of bioinorganic and biomimetic chemistry, generous host, and an inspirational scientific leader full of energy and contagious enthusiasm. AR thanks the European Commission for an Erasmus Mundus predoctoral fellowship. GCL thanks the Wenner-Gren Foundation for a visiting researcher fellowship to Lund University.

Appendix B. Supplementary material

Supplementary data to this article, can be found online at https:/doi.org/…. CCDC entries no 2224424, 2225168, 2,224,198 contain the supplementary crystallographic data for **2**, **3** and **8**, respectively. Copies of this information may be obtained free of charge from The Director,

CCDC, 12 Union Road, Cambridge, CB2 1EZ, UK (fax: +44–1223-336,033; e-mail: deposit@ccdc.cam.ac.uk or http://www.ccdc.cam.ac.uk).

References

[1] R. Cammack, M. Frey, R. Robson (Eds.), Hydrogen as a Fuel, CRC Press, 2001.
[2] T.R. Simmons, G. Trevor, M. Berggren, M. Bacchi, V. Fontecave, Artero, Coord. Chem. Rev. 270 (2014) 127–150.
[3] W. Lubitz, H. Ogata, O. Rüdiger, E. Reijerse, Chem. Rev. 114 (2014) 4081–4148.
[4] R. Grinter, A. Kropp, H. Venugopal, M. Senger, J. Badley, P.R. Cabotaje, R. Jia, Z. Duan, P. Huang, S.T. Stripp, C.K. Barlow, M. Belousoff, H.S. Shafaat, G.M. Cook, R.B. Schittenhelm, K.A. Vincent, S. Khalid, G. Berggren, C. Greening, Nature 615 (2023) 541–547.
[5] M. Stephenson, L.H. Stickland, J. Biochem. 25 (1931) 205.
[6] R.K. Thauer, A.R. Klein, G.C. Hartmann, Chem. Rev. 96 (1996) 3031.
[7] J.W. Peters, W.N. Lanzilotta, B.J. Lemon, L.C. Seefeldt, Science 282 (1998) 1853.
[8] J.H. Artz, O.A. Zadvornyy, D.W. Mulder, S.M. Keable, A.E. Cohen, M.W. Ratzloff, S. G. Williams, B. Ginovska, N. Kumar, J. Song, S.E. McPhillips, C.M. Davidson, A. Y. Lyubimov, N. Pence, G.J. Schut, A.K. Jones, S.M. Soltis, M.W.W. Adams, S. Raugei, P.W. King, J.W. Peters, J. Am. Chem. Soc. 142 (2020) 1227–1235.
[9] M. Bruschi, C. Greco, P. Fantucci, L. De Gioa, Inorg. Chem. 47 (2008) 6056.
[10] B.J. Lemon, J.W. Peters, Biochemistry 38 (1999) 12969.
[11] Y. Li, T.B. Rauchfuss, Chem. Rev. 116 (2016) 7043–7077.
[12] B.E. Barton, M.T. Olsen, T.B. Rauchfuss, J. Am. Chem. Soc. 130 (2008) 16834–16835.
[13] D. Chouffai, G. Zampella, J.F. Capon, L. De Gioia, F. Gloaguen, F.Y. Pétillon, P. Schollhammer, J. Talarmin, Inorg. Chem. 50 (2011) 12575–12585.
[14] A. Rahaman, S. Gosh, D.G. Unwin, S. Basak-Modi, K.B. Holt, S.E. Kabir, E. Nordlander, M.G. Richmond, G. Hogarth, Organometallics 33 (2014) 1356–1366.
[15] L. Hongxiang, T.B. Rauchfuss, J. Am. Chem. Soc. 124 (2002) 726–727.
[16] S. Ghosh, A. Rahaman, G. Orton, G. Gregori, M. Bernat, U. Kulsume, N. Hollingsworth, K.B. Holt, S.E. Kabir, G. Hogarth, Eur. J. Inorg. Chem. 42 (2019) 4506–4515.
[17] A. Rahaman, C.G. Suriñach, A. Ficks, G.E. Ball, M. Bhadbhade, M. Haukka, L. Higham, E. Nordlander, S.B. Colbran, Dalton Trans. 46 (2017) 3207.
[18] S. Ghosh, A. Rahaman, K.B. Holt, E. Nordlander, M.G. Richmond, S.E. Kabir, G. Hogarth, Polyhedron 116 (2016) 127–135.
[19] A.K. Jones, E. Sillery, S.P.J. Albracht, F.A. Armstrong, Chem. Commun. 8 (2002) 866–867.
[20] J. Windhager, M. Rudolph, S. Bräutigam, H. Görls, W. Weigand, Eur. J. Inorg. Chem. 18 (2007) 2748–2760.
[21] C.A. Tolman, Chem. Rev. 77 (1977) 313–348.
[22] A. Rahaman, Ph.D. Thesis, Lund University (2016).
[23] K. Morita, S. Kobayashi, Chem. Pharm. Bull. 15 (1967) 988–993.
[24] D. Liang, J. Bian, L.W. Deng, D. Huang, J. Funct. Foods 35 (2017) 197–204.
[25] A. Shaver, P.J. Fitzpatrick, K. Steliou, I.S. Butler, J. Am. Chem. Soc. 101 (1979) 1313–1315.
[26] CrysAlisPro Agilent, Agilent Technologies Inc., Yarnton, Oxfordshire, England, (2014).
[27] G.M. Sheldrick, Crystal structure refinement with SHELXL, Acta Cryst. C71 (2015) 3–8.
[28] L.C. Song, Z.Y. Yang, Y.J. Hua, H.T. Wang, Y. Liu, Q.M. Hu, Organometallics 26 (2007) 2106–2110.
[29] W. Hieber, J. Gruber, Z. Anorg. Allg. Chem. 296 (1958).
[30] S. Rana, S. Ghosh, M.K. Hossain, A. Rahaman, G. Hogarth, S.E. Kabir, Trans. Met. Chem. 41 (2016) 933–942.
[31] S. Ghosh, G. Hogarth, N. Hollingsworth, K.B. Holt, I. Richards, M.G. Richmond, B. E. Sanchez, D.G. Unwin, Dalton Trans. 42 (2013) 6775–6792.
[32] G. Hogarth, S.E. Kabir, I. Richards, Organometallics 29 (2010) 6559–6568.
[33] J.F. Capon, F. Gloaguen, F.Y. Pétillon, P. Schollhammer, J. Talarmin, Eur. J. Inorg. Chem. 30 (2008) 4671–4681.
[34] X.F. Liu, Z.Q. Jiang, Z.J. Jia, Polyhedron 33 (2012) 166–170.
[35] S. Ghosh, G. Hogarth, N. Hollingsworth, K.B. Holt, S.E. Kabir, B.E. Sanchez, Chem. Commun. 50 (2014) 945–947.
[36] J.M. Camara, T.B. Rauchfuss, Nat. Chem. 4 (2012) 26–30.
[37] J.M. Camara, T.B. Rauchfuss, J. Am. Chem. Soc. 133 (2011) 8098–8101.
[38] L. Song, C. Li, J. Ge, Z. Yang, H. Wang, J. Zhang, Q. Hu, J. Inorg. Biochem. 102 (2008) 1973–1979.
[39] S. Kaur-Ghumaan, A. Sreenithya, R.B. Sunoj, J. Chem. Sci. 127 (2015) 557–563.
[40] P. Li, M. Wang, C. He, G. Li, X. Liu, C. Chen, B. Åkermark, L. Sun, Eur. J. Inorg. Chem. (2005) 2506–2513.
[41] L. Song, Q. Li, Z. Yang, Y. Hua, H. Bian, Q. Hu, Eur. J. Inorg. Chem. 7 (2010) 1119–1128.
[42] F.I. Adam, G. Hogarth, I. Richards, J. Org. Met. Chem. 692 (2007) 3957–3968.
[43] F.I. Adam, G. Hogarth, S.E. Kabir, D. Richards, Comptes, Rev. Chim. 11 (2008) 890–905.
[44] L. Schwartz, G. Eilers, L. Eriksson, A. Gogoll, R. Lomoth, S. Ott, Chem. Commun. (2006) 520–522.
[45] I.P. Georgakaki, M.L. Miller, M.Y. Darensbourg, Inorg. Chem. 42 (2003) 2489–2949.
[46] P.H. Zhao, M.Y. Hu, J.R. Li, Y.Z. Wang, B.P. Lu, H.F. Han, X.F. Liu, Electrochim. Acta 353 (2020) 136615.
[47] M.Y. Hu, L. Yan, J.R. Li, Y.H. Wang, P.H. Zhao, X.F. Liu, Appl. Organometal. Chem. 33 (2019) 4949.
[48] S. Ezzaher, J.F. Capon, F. Gloaguen, F.Y. Pétillon, P. Schollhammer, J. Talarmin, N. Kervarec, Inorg. Chem. 48 (2009) 2–4.
[49] N. Wang, M. Wang, J. Liu, K. Jin, L. Chen, L. Sun, Inorg. Chem. 48 (2009) 11551–11558.
[50] S. Ezzaher, J.F. Capon, N. Dumontet, F. Gloaguen, F.Y. Pétillon, P. Schollhammer, J. Talarmin, Electroanal. Chem. 626 (2009) 161–170.
[51] S. Ezzaher, J.F. Capon, F. Gloaguen, F.Y. Pétillon, P. Schollhammer, J. Talarmin, Inorg. Chem. 46 (2007) 3426–3428.
[52] S. Ghosh, B.E. Sanchez, I. Richards, M.N. Haque, K.B. Holt, M.G. Richmond, G. Hogarth, J. Organomet. Chem. 812 (2016) 247–258.
[53] S. Ezzaher, J.F. Capon, F. Gloaguen, F.Y. Pétillon, P. Scholhammer, J. Talarmin, Inorg. Chem. 46 (2007) 9863–9872.
[54] W. Gao, J. Ekström, J. Liu, C. Chen, L. Eriksson, L. Weng, B. Åkermark, L. Sun, Inorg. Chem. 46 (2007) 1981–1991.
[55] G.A.N. Felton, C.A. Mebi, B.J. Petro, A.K. Vannucci, D.H. Evans, R.S. Glass, D. L. Lichtenberger, J. Organomet. Chem. 694 (2009) 2681–2699.
[56] R. Mejia-Rodriguez, D. Chong, J.H. Reibenspies, M.P. Soriaga, M.Y. Darensbourg, J. Am. Chem. Soc., 126 (2004) 12004–12014.
[57] S. Ghosh, S. Basak-Modi, M.G. Richmond, E. Nordlander, G. Hogarth, Inorg. Chim. Acta 480 (2018) 47–53.
[58] D. Chong, I.P. Georgakaki, R. Mejia-Rodriguez, J. Sanabria-Chinchilla, M. P. Soriaga, M.Y. Darensbourg, Dalton Trans. 21 (2003) 4158–4163.
[59] G.A. Felton, A.K. Vanucci, J. Chen, L.T. Locket, N. Okumura, B.J. Petro, U.I. Zakai, D.H. Evans, R.S. Glass, D.L. Lichtenberger, J. Am. Chem. Soc. 129 (2007) 12521–12530.
[60] Y.C. Liu, K.T. Chu, R.L. Jhang, G.H. Lee, M.H. Chiang, Chem. Commun. 49 (2013) 4743–4745.
[61] S. Ghosh, S. Rana, N. Hollingsworth, M.G. Richmond, S.E. Kabir, G. Hogarth, Inorganics 6 (2018) 122.
[62] D.G. Unwin, S. Ghosh, F. Ridley, G.M. Richmond, K.B. Holt, G. Hogarth, Dalton Trans. 48 (2019) 6174–6190.
[63] A. Jablonskytė, L.R. Webster, T.R. Simmon, J.A. Wright, C.J. Pickett, J. Am. Chem. Soc. 36 (2014) 13038–13044.
[64] S. Ghosh, N. Hollingsworth, M. Warren, D.A. Hrovat, M.G. Richmond, G. Hogarth, Dalton Trans. 48 (2019) 6051–6060.
[65] F. Gloaguen, J.D. Lawrence, T.B. Rauchfuss, M. Bénard, M.M. Rohmer, Inorg. Chem. 41 (2002) 6573–6582.
[66] F. Gloaguen, J.D. Lawrence, T.B. Rauchfuss, J. Am. Chem. Soc. 123 (2001) 9476–9477.